Stockholm University

Master Thesis

Degree Project in
Marine Geology 60 hp

Holocene Burial of Terrestrial Organic Matter in the Mackenzie Trough, Canadian Arctic

Daniel Rudbäck

Stockholm 2023

Department of Geological Sciences
Stockholm University
SE-106 91 Stockholm

Abstract

Circum-arctic permafrost soil hosts almost half of the global shallow soil carbon inventory, exceeding the amount of carbon currently stored in the atmosphere. Global warming has Arctic temperatures increasing 4 times faster than the global average, threatening to remobilise this carbon. This can reinforce a positive feedback loop between increasing atmospheric CO_2 concentrations and further warming, and potentially lead to acidification of coastal waters. Determining the fate of remobilised terrestrial carbon is key to understanding the effect of thawing permafrost on the global climate. The Mackenzie River transports a large quantity of terrestrial carbon to the Mackenzie delta and eventually the Beaufort Shelf. The current understanding is that a majority of the remobilised carbon is efficiently buried in the delta and on the shelf. However, this assertion is based on a carbon budget constructed 25 years ago with limited spatial data on the actual fluxes and lacking clear distinctions between the sources and types of buried organic matter. This study focuses on organic carbon entering the Mackenzie Trough, an area of the shelf not included in the original budget where an estimated 42% of riverine sediments are deposited. Using a diverse methodology of organic and inorganic geochemistry, radioisotope analysis and endmember modelling, further evidence is presented for a high burial efficiency of OC in offshore sediments. In addition, the results of this study uncover a correlation between petrogenic POC and silt-sized sediments, which suggests that offshore sediment transport processes play an important role in the distribution and burial of OC from different terrestrial carbon pools.

Table of Contents

1.0 Introduction

Permafrost coasts account for approximately 34% of the world's coastlines with 25% directly bordering the Arctic Ocean (Lantuit et al., 2012). The northern permafrost zone makes up 16% of global soil area, and contains 1035 ± 150 Pg of carbon in the upper 3 meters, where it is stored over millennial timescales (Hugelius et al., 2014; Tarnocai et al., 2009). Global estimates for carbon in the top 3 meters of soil are 2344 Pg, implying that the northern permafrost zone contains approximately 44% of the global surface soil carbon inventory (Jobbágy and Jackson, 2000). The amount of carbon in northern permafrost exceeds the 875 Pg carbon found in the atmosphere (Friedlingstein et al., 2022), and is at risk of being released to the oceans and atmosphere as climate change accelerates warming in the Arctic.

The storage of carbon in soils is an important sink for atmospheric CO_2. Photosynthesizing plants turn atmospheric CO_2 into organic matter, and subsequentially expire, leaving their remains to be oxidized and re-used. Over time, a fraction of this organic matter will avoid oxidation, and instead be stored in the soil (Batjes, 1996). In the case of permafrost, relatively fresh organic material can be frozen in the host soil for thousands of years (Schuur et al., 2015). However, Arctic air temperatures are warming almost four times faster than the global average (Rantanen et al., 2022) and the high latitudes are experiencing dramatic changes as an effect of this polar amplification of climate change.

Increased temperatures are thawing permafrost, resulting in previously frozen carbon stocks being exposed to processes in the active layer. Here it becomes susceptible to oxidation by microbes – releasing CO_2 or CH_4 in the process; or to erosion – being released directly to coastal waters or transported by rivers and streams (Hilton et al., 2015; Schuur et al., 2015). If the carbon avoids oxidation during fluvial transport, it ends up in the ocean. Here, a fraction is buried in marine sediments, where it can potentially be stored for tens of thousands of years - essentially being transferred from the shorter-term storage in permafrost to the longer-term storage in marine sediments (Hilton et al., 2015).

Estimating how much remobilised carbon is delivered to the oceans and buried offshore is challenging. Large uncertainties exist in concerning the rate at which thawed soil is eroded into rivers, the oxidation of carbon during transport, the burial efficiency in marine sediments, and how all these processes change over large spatial scales. Numerous studies on marine burial of organic carbon from thawing permafrost exist across the Arctic (Macdonald et al., 1998; Vonk et al., 2014; Hilton et al., 2015; Martens et al., 2019; Kim et al., 2022), as well as a database for the abundance, and isotopic composition ($\delta^{13}C$, $\Delta^{14}C$) of organic carbon in Arctic marine sediments (Martens et al., 2021). However, substantial spatial gaps exist in the available surface measurements, and few reported sedimentation rates exist for many regions of the Arctic, making it difficult to accurately determine burial rates of OC offshore.

Organic carbon in Arctic shelf sediments originates from several sources, which can be partially fingerprinted using geochemical mixing models if endmembers can be identified and characterized. Common geochemical properties used for source appointment include $\delta^{13}C$, $F^{14}C$ and the C/N ratio. $F^{14}C$, or sometimes F_{mod}, is a conversion of the $\Delta^{14}C$ value representing a fractional value between modern ($\Delta^{14}C$ = 0‰, $F^{14}C$ = 1) and ancient or radiocarbon dead ($\Delta^{14}C$ = 1000‰, $F^{14}C$ = 0). These values, and the associated age relate to one another by the following equations:

(1) $$\Delta^{14}C = \left[F^{14}C * e^{\lambda(1950-Y_c)} - 1\right] * 1000$$

(2) $$Age\ (Cal\ yrs\ BP) = -8033 * \ln(F^{14}C)$$

where λ is the inverse mean-life of radiocarbon (1/8267) and Y_c is the year of collection (Stuiver and Polach, 1977). More specific methods for source fingerprinting employ compound specific properties such as the concentration of lignin phenols, or the ratio between specific hydroxy acids and phenols (Bröder et al., 2018, 2016; Kim et al., 2022).

Sources of organic carbon in Arctic shelf sediments commonly include A) marine primary production, B) freshwater primary production, C) recent terrestrial vegetation and D) shallow and deep soils. Yedoma is another commonly identified source, it is an ice-rich silt deposit containing aged ($\Delta^{14}C$: -945.6 ± 66.4 ‰) organic carbon (site-specific averages of 1.2 – 4.8 wt.%) formed during the late Pleistocene in Beringia (Siberia, Alaska and Yukon) (Behnke et al., 2023; Schirrmeister et al., 2013). In the Mackenzie drainage basin, a petrogenic source of organic carbon is

also recognised as being important. This endmember consists of ancient OC (radiocarbon dead), such as kerogens, hosted in sedimentary or meta-sedimentary bedrock in the form of coal or shales (Campeau et al., 2020).

On the Beaufort Shelf, 4 main sources for OM are commonly identified; A) marine primary production, B) freshwater primary production, C) recent terrestrial vegetation and young soils, as well as D) ancient petrogenic carbon (Behnke et al., 2023). Differentiating between these sources is complicated as characteristic geochemical signatures overlap, and considerable variability exists in how these different endmembers are defined in the literature (Fig. 1). However, differentiating between endmembers is important as the OC from different sources vary in their susceptibility to mineralisation. Furthermore, documenting changing sources through time informs about how climate change is altering the terrestrial-marine carbon system.

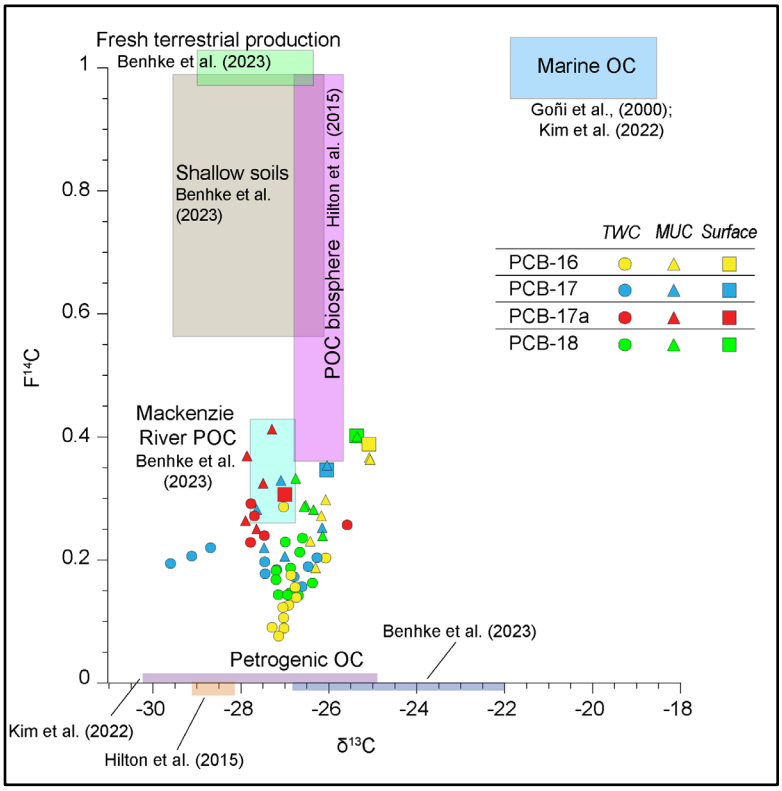

Figure 1. F14C (Y-axis) and 13C (X-axis) of samples from this study, distinguished by the type of sample (TWC/GC, MUC and sediment-surface sample). The coloured fields represent the values of various endmembers found in literature.

The most comprehensive estimate for OC burial in the Canadian Beaufort Sea was published over 25 years ago (MacDonald et al., 1998), and has remained the most cited carbon budget for this region of the Arctic. Macdonald et al. (1998) estimated that 2.1 ± 0.3 Mt of terrestrial particulate organic carbon (POC) is delivered by the Mackenzie River each year, of which 1.21 Mt makes it past the delta and onto the shelf. The burial of organic carbon is estimated to be 1.95 ± 0.5 Mt per year, of which 1.07 ± 0.4 is buried in the delta, and 0.71 ± 0.3 is buried on the shelf (Fig. 2).

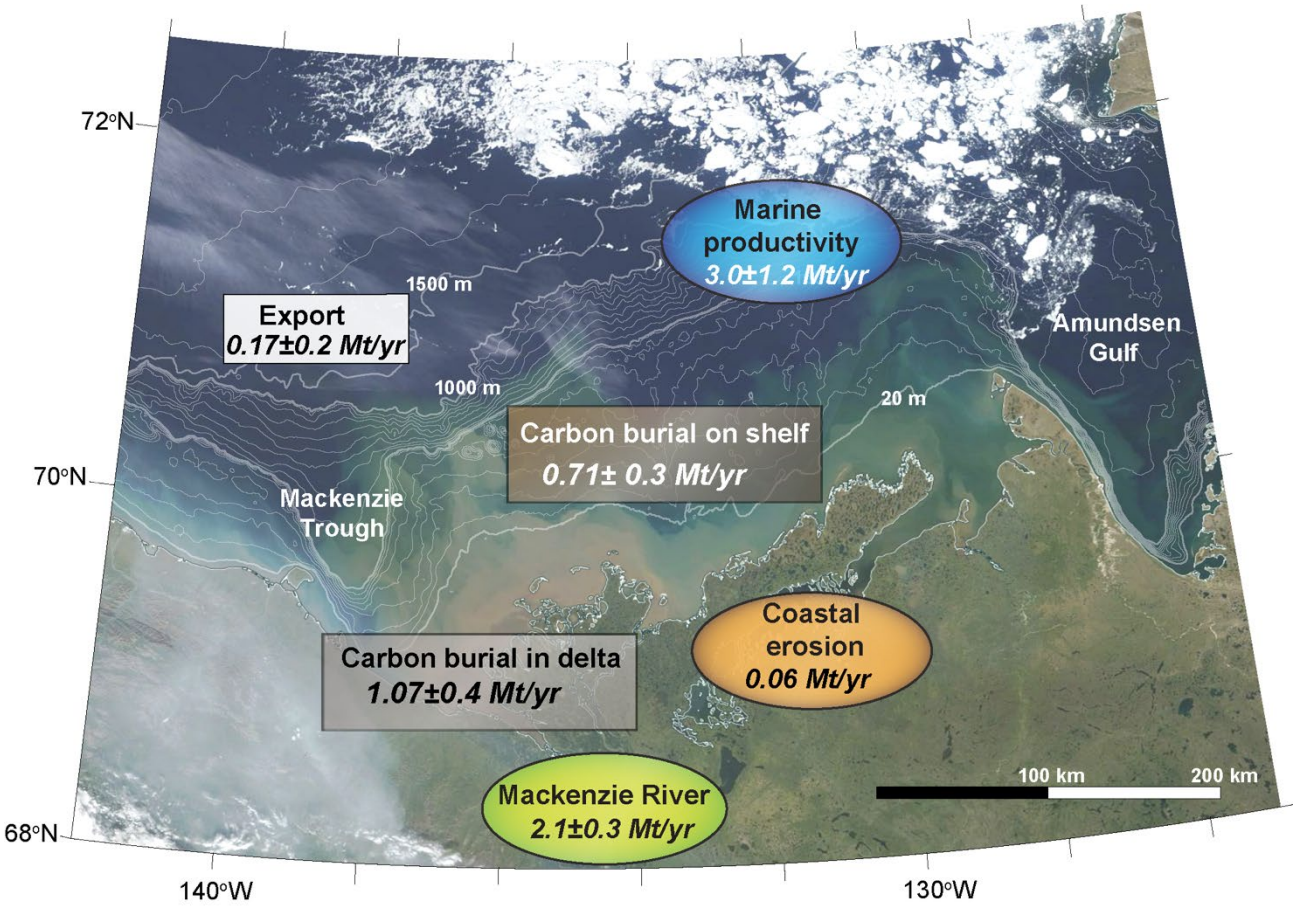

Figure 2. A visualization of the carbon budget for Mackenzie River, Delta and the Beaufort Shelf from Macdonald et al. (1998).

Macdonald et al. (1998) argue that more than 90% of this carbon is refractory and of terrestrial origin, meaning that the far more bioavailable marine organic carbon is preferentially recycled in the water column or at the seafloor. After accounting for an estimated 20% loss to oxidation in surface sediments, the authors conclude that about 60% of POC delivered by the Mackenzie River outflow and coastal erosion is buried in the delta or on the shelf. Less than 30% is estimated to be transported further offshore, escaping the shelf, while the remaining carbon is oxidized or metabolized. The 20% loss due to oxidation after post-deposition is not well motivated and is based on estimates for sediments in the delta, not the shelf. Removing this loss from their calculations results in 1.7 Mt of terrestrial POC, out of the total 2.1 Mt delivered by the Mackenzie River being buried in delta- and shelf sediments, or just over 80%.

At the time of publication, the authors acknowledged several limitations to this budget, one of which is the fact OC burial in the Mackenzie Trough is omitted. This is a potentially large catchment for OC burial, as it is estimated that 42% of river borne sediments that pass the delta end up in the Mackenzie Through, one of the areas with the highest sediment accumulation rates on the Beaufort Shelf (Harper and Penland, 1982; Macdonald et al., 1998). It was not included in the original budget as there were no available measurements for the sedimentation rate in the Mackenzie Trough at the time. In fact, the study only used estimates of the sedimentation rate for shelf areas shallower than 100 m, where it was possible to estimate the sediment thickness overlying the Holocene transgressive surface using geophysical data (Macdonald et al., 1998). This postglacial transgression surface was not possible to identify in the Mackenzie Trough.

One of the conclusions drawn from the original OC budget was that there was a general balance between delivery and burial of terrigenous OC on the Beaufort Sea shelf. However, both Mackenzie river discharge, and the mass of sediments delivered by the river, has increased significantly over the past decades. Doxaran et al., (2015) concluded that between 2003 and 2013, river discharge increased by 22% accompanied by an increase in suspended particulate matter (SPM) – the sediment load – by 46%. Their work also highlighted a notable discrepancy between the satellite-derived estimates of suspended particulate matter and the field-based estimates of Macdonald et al. (1998). Although the discharge and sediment load have greatly increased in the timespan between the studies, satellite-based estimates presented by Doxaran et al. (2015) are smaller than those estimated by Macdonald et al. (1998) by a factor of between 2 and 6, depending on how Doxaran et al. (2015) extrapolate their data to fit a longer timeframe. Therefore, while Macdonald et al. (1998) argued that there was a general balance between OC delivery to the shelf and offshore burial, major gaps in the spatial coverage for offshore burial rates exist and this inferred balance is more generally questioned by modern observations on the magnitude and rate of change for terrigenous OC delivery.

Improving estimates of the amount, source and burial rates of terrestrial OC in the Canadian Beaufort Sea was the overarching objective of the 2021 *Permafrost Carbon in the Beaufort Sea* (PeCaBeau) expedition on the Canadian Coast Guard Vessel *Amundsen* (Bröder et al., 2022). During this 4-week expedition, 27 sediment cores were collected from 5 cross-shelf transects (Fig. 3), including 4 coring stations on a transect through the Mackenzie Trough. In addition, multicores were collected from 26 stations.

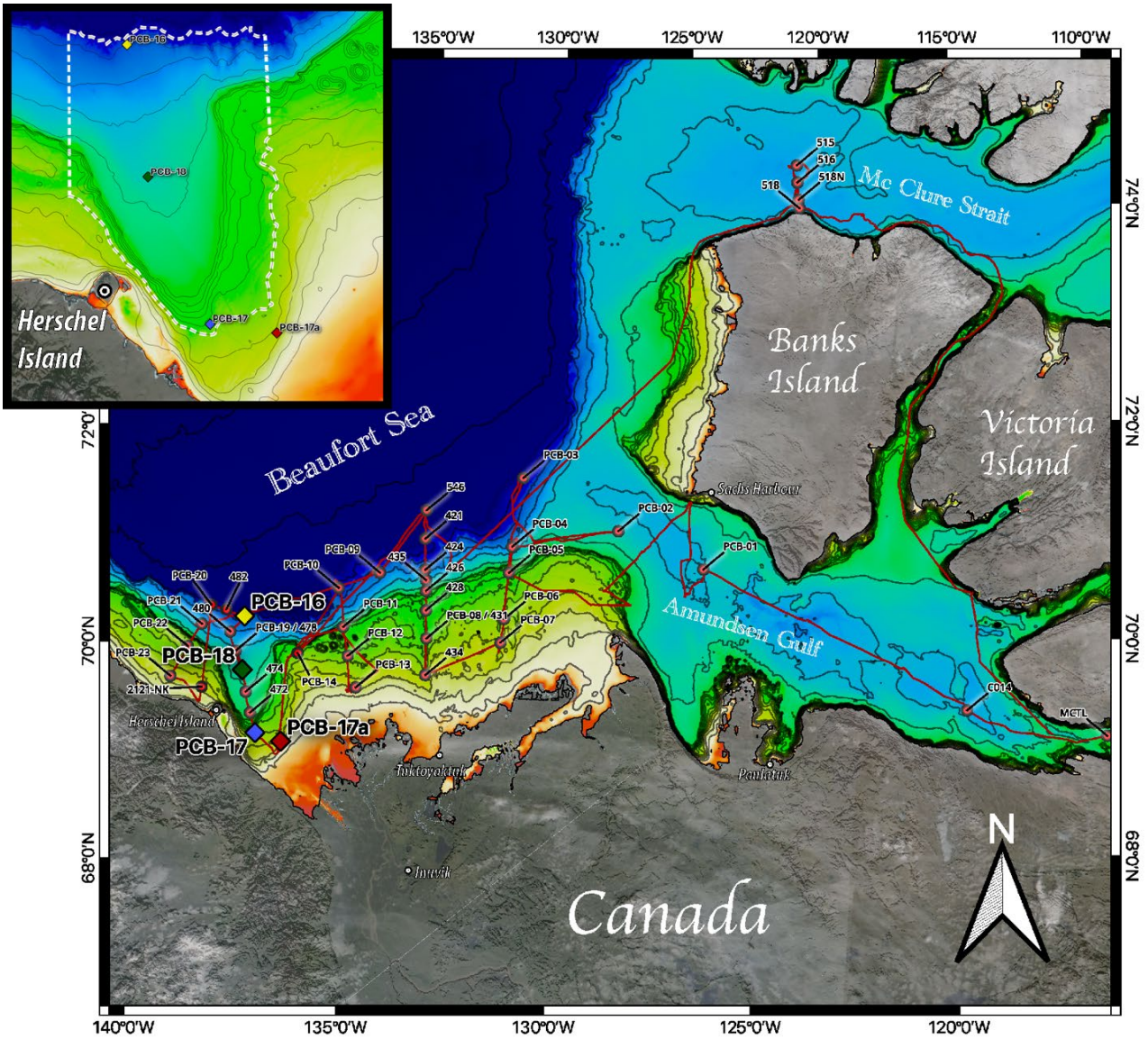

Figure 3. Bathymetry of the Canadian Beaufort Sea featuring the ship-track and sampling stations of the PeCaBeau expedition in 2021. The magnified figure displays Mackenzie Trough (outlined by the dashed white line) and the coring-sites from this study.

In this project a transect of sediment cores from the Mackenzie Trough are investigated to determine the rate of organic matter burial, what proportion of this is derived from terrestrial sources, and whether this has changed through the Holocene. Three hypotheses are tested:

1. The Mackenzie Trough is a significant sink for remobilised terrestrial OC that can potentially balance observed rates of increased POC delivery from river discharge and coastal erosion.

2. Moving offshore, compositional and isotopic proxies used to partition sources of organic material (i.e. $\delta^{13}C$, $\Delta^{14}C$, N/[OC], Al/[OC]) will show a larger input of marine organic matter and less influence from river derived biogenic and petrogenic sources.

3. Accumulation rates and relative contributions of different OC sources have remained constant through the late Holocene.

2.0 Methods

2.1 Physiography and Area of the Mackenzie Trough

The Mackenzie Trough is a northwest trending bathymetric depression that divides the 50,000 km^2 Canadian Beaufort Shelf into the eastern and western sectors. It lies seaward of the modern Mackenzie Delta and intersects the shelf break at a depth of 400 mbsl (Fig. 3). It formed as a glacially excavated valley (Blasco et al., 1990; Shearer, 1971) and has a base defined by a smooth, U-shaped erosional unconformity overlying Miocene sediments in the central trough, and Plio-Pleistocene sediments on the flanks (Dietrich et al., 1989).

In this study, the area of the Mackenzie Trough was defined by the 50 m and the 1000 m isobaths. The deeper isobath was selected based on a break in the slope at the seaward end of the trough, where it steps steeply down into the Amerasian Basin. Longitudinal limits were set at -139.5°E and -137.25°E in the WGS 84 / IBCAO Polar Stereographic coordinate reference system. The ellipsoidal area was calculated using GIS and found to be 9,151,974,568 m^2 , or 9152 km^2.

2.2 Sample collection & subsampling

The samples were collected using different coring tools. These included a piston-corer (PC) often with an accompanying trigger weight core (TWC), a gravity-corer (GC) and a multi-corer (MC) to acquire intact sediments from at and immediately below, the seafloor. Shipboard measurements of bulk density and magnetic susceptibility were made on all PC's, GC's, TWC's, and an archived MC using a Geotek Multi-Sensor Core Logger (MSCL). Four sites were analysed in this study, 3 lying within the Mackenzie Trough (PCB-16,18, 17) and 1 found just landward (PCB-17a) (Table 1).

Core name	Latitude (DD)	Longitude (DD)	Water depth (m)	Core length (cm)
PCB-16-GC	70.50464	-138.83203	778	269
PCB-17-TWC	69.43113	-137.99893	54	232.5
PCB-17a-GC	69.28782	-137.27927	19	124.5
PCB-18-TWC	69.99839	-138.62824	268	288.5
PCB-16-MUC	70.50464	-138.83203	778	43
PCB-17-MUC	69.43113	-137.99893	54	48.5
PCB-17a-MUC	69.28782	-137.27927	19	27.5
PCB-18-MUC	69.99839	-138.62824	268	42
PCB-16-GGC	70.50464	-138.83203	778	350.5
PCB-17-PC	69.43113	-137.99893	54	327
PCB-18-PC	69.99839	-138.62824	268	682

Table 1. Core names, coordinates, water depth and lengths for the primary cores of this study, multicores as well as cores from the same stations not analysed in this study.

Multi-cores were cut into 1-2 cm thick slices and frozen shipboard. Subsampling of the TWC's also occurred shipboard, with 38 samples extracted by drilling a 1 cm diameter hole into the core liner and pushing a syringe with its top cut off into the sediment. 8 cm^3 of sediment were removed and placed into plastic bags and frozen. These samples are referred to as "*syringe samples*". All frozen samples were shipped to ETH-Zurich where they were freeze-dried. Most of the longer Piston and Gravity cores were shipped to AWI-Potsdam for long-term storage. In December 2021 and February 2022 sampling parties were organised in Potsdam where these cores were split, described and sampled. U-channels were taken from them and later run on an ITRAX XRF-core scanner at Stockholm University. One half of each section was preserved as an archive, while the other was cut into 1-2 cm slices before being frozen.

Subsamples were used for radiocarbon dating of the organic fraction, radionuclide measurements for dating, bulk organic parameters, ICP-OES and grain size (Table 2). A correlation analyses of the grain size, elemental abundances, and organic matter properties was performed using the packages "stats" and "corrplot" for R-Studio, to investigate predictive relationships and processes controlling organic matter deposition.

Sample suite	**Grain size**	**Elemental Analyses**	**^{14}C, TOC, C/N**	**^{15}N, ^{13}C**	**^{210}Pb, ^{137}Cs**
Syringe samples (bulk)	✓				
Syringe samples (<63 µm)		✓	✓	✓	
Multicore samples			✓	✓	✓

Table 2. Sample suites and associated analyses.

2.3 ^{210}Pb/^{137}Cs radioisotope dating and age modelling.

Radioisotope dating of multicore samples was performed at the Swedish Museum of Natural History in Stockholm, Sweden. A DSPEC Digital Gamma Ray Spectrometer from EG&G ORTEC was used

with a germanium detector running at 4000 V, cooled by liquid nitrogen. The software used was Maestro Pro. The samples were homogenised with a pestle and mortar before placing approximately 10 g of sample inside of plastic containers which were sealed by Parafilm and allowed to equilibrate for 4 weeks before analysis. Samples spent either 2 or 3 days running on the instrument. The gamma ray peaks were calibrated by running known samples of ^{241}Americium and ^{137}Caesium, and the efficiency was calibrated using a sample of generic marine sediment spiked with Uraninite from Stackebo, Sweden (in secular equilibria), with a known activity of ^{238}U (Measured and calculated at the Swedish Museum of Natural History in 2003).

Sediment accumulation rates (SAR) were calculated with 'serac' in R, using the excess ^{210}Pb in a constant flux constant supply (CFCS) model (Bruel and Sabatier, 2020). The resulting estimate for the year 1960 was compared to the appearance of ^{137}Cs in the sediment, to assure that the model's result was reasonable. Linear sedimentation rates derived from the radionuclide measurements were extrapolated to the base of each core, and must later be refined using other dating approaches (i.e. ^{14}C of foraminfera or mollusc shells and/or paleomagentic secular variation).

2.4 Grain size and grain density

The grain size was measured on syringe samples using a Malvern Panalytical Mastersizer 3000 laser particle size analyser, with the Hydro LV wet dispersion unit. Prior to analysis, the samples were gently broken up by hand while inside the sample bag. Samples were then added to the dispersion unit, pre-prepared with 3 ml of sodium hexametaphosphate ($Na_6[(PO_3)_6]$) as a dispersing agent, until an obscuration of 5-15% was reached. After 3 minutes of stirring and sonication, the analysis was initiated. Each sample was measured a minimum of 5 times, using the resulting average value with GRADISTAT (Blott and Pye, 2001) for statistical analysis and classification of the grain sizes. Between each sample the instrument's self-cleaning cycle was used to rinse away any remaining sample. After the multi-core samples had been measured on the gamma-detector, the grain density was measured on a Micromeretics Accupyc helium displacement pycnometer. Roughly 10 g of dry and ground sediment was placed in the sample vial, and an average volume from 5 cycles was used to calculate the dry density of the material.

2.5 Organic matter analyses

Following the work of Hilton et al (2015) on a borehole at the landward end of the Mackenzie Trough, we attempted to separate and date the fine and coarse fraction components of the OC. Samples were weighed and placed in Erlenmeyer flasks. A small amount of de-ionized water was added before they were placed on a stirring table for 2 hours to rehydrate and disaggregate. The wet sediments were then sieved through a 63µm sieve, retaining the fine-grained fraction in freezer bags. The coarse-grained fractions were dried and stored in glass vials. The fine-grained fraction material was then frozen and allowed to thaw overnight in order to promote sedimentation. Following this, the supernatant was removed with a vacuum-pipette before the samples were freeze-dried. Ultimately there was too little coarse faction material to date separately, and this material has been stored long-term for potential future analyses.

The fine-grained fraction ranged between 1-2 g dry weight (depending on the original size of sample). These samples were shipped to the Laboratory of Ion Beam Physics at ETH Zürich, Switzerland where they were analysed for total organic carbon content (TOC) as well as for stable nitrogen and carbon isotopes and radiocarbon.

Subsamples of approximately 20 mg were acid fumigated with 37% HCL for 72 hours at 60°C to remove inorganic carbon before neutralizing and drying the subsamples over sodium hydroxide (NaOH) at 60°C for another 72 hours.

TOC and radiocarbon were measured with an online elemental analyser (EA) accelerator mass spectrometry (AMS) system (EA: vario MICRO cube, Elementar; AMS: Mini Carbon Dating System MICADAS, Ionplus, Dietikon, Switzerland). A detailed methodology can be found in (Ruff et al., 2010). The radiocarbon is reported in accordance with (Stuiver and Polach, 1977).

Stable isotopes were measured with an EA coupled to an isotope ratio mass spectrometer (EA: vario MICRO cube, Elementar; IRMS: Isoprime) and were reported in $\delta^{13}C$ notation relative to the international standard VPDB (Vienna PeeDee Belemnite).

2.6 ICP-OES of major elements

The elemental composition was analysed at the Stable Isotope Laboratory (SIL) at Stockholm University on the fine-grained fraction from syringe samples. First, the samples were washed to remove salt. 1 g of dry sample was added to a 15 ml centrifuge vial. Milli-Q water was added to the 10 ml mark. The samples were shaken and vortexed before being centrifuged at 4200 rpm for 15 minutes. The supernatant was removed, and the process was repeated, only this time the samples were placed on a stirring table overnight, to resuspend the sediment.

Following cleaning, the samples were freeze dried before continuing preparation. 100 mg of sample was weighed out together with 150 mg lithium metaborate ($LiBO_2$ $2H_2O$) before being homogenised in an agate pestle and mortar. The sample was then transferred to a graphite crucible with a cone-shaped bottom and the crucible was placed in an oven at 1000 degrees for 4 hours, before allowing the oven to cool to room-temperature overnight.

The next day, the resulting melt was transferred to 100 ml plastic bottles, and 25 ml 8% nitric acid (HNO_3) was added. The plastic bottles were placed on a stirring table overnight, to allow the melt to completely dissolve. The following day the samples were gravity-filtered through Munktell 00M ashless filter papers into 100 ml volumetric flasks, and Milli-Q water was added to the 100 ml mark. The samples were then analysed by inductively coupled plasma optical emission spectroscopy (ICP-OES) on a Thermo Scientific iCAP 6000 series with a Cetac ASX-520 AutoSampler attached. The standards used were geological reference materials JSD-1 from the Geological Survey of Japan as well as NCS DC 70311 and NCS DC 70314 from NCS Testing Technology Co., Ltd.

2.7 Endmember modelling of OC sources

Different approaches were applied for source partitioning of OC using end-member modelling. An endmember mixing model for $\delta^{13}C$ was written in R, where a simple weighted average calculation is performed that assumes each sample is the average of the two endmembers with different weights:

(3) $$\delta^{13}C_{sample} = \delta^{13}C_{EM1} * X + \delta^{13}C_{EM2} * (1 - X)$$

(4) $$X = \frac{\delta^{13}C_{sample} - \delta^{13}C_{EM2}}{\delta^{13}C_{EM1} - \delta^{13}C_{EM2}}$$

where *X* is the resulting ratio of EM1, while *(1-X)* is the ratio of EM2.

A Monte-Carlo simulation was applied (n=1000) to the endmember values, by generating random numbers in a normal distribution using the SD of the endmember values. To ensure that the calculated values are reasonable, any solution with EM >1 is rejected. Output from the script presents the data as an average ratio, the SD of all the iterations, and the number of accepted values. Two different dual isotope end-member models ($\delta^{13}C$ and $F^{14}C$) were also applied to the data using a MATLAB script originally published by (Bosch et al., 2015) and modified by Philip Pika and later by C. Stranne at Stockholm University. When modelling the $F^{14}C$, the $\Delta\Delta^{14}C$ (delta-delta) is calculated and used for the samples. This means that the extrapolated sediment age (from the radioisotope age model) is subtracted from the $F^{14}C$ age, which results in an estimate of the difference between the depositional age and the age of the OC that is used in the end-member modelling.

3.0 Results

3.1 Core lithology

The sediments are generally olive green, with site-average bulk densities ranging from 1.47 g/cm^3 furthest from shore (PCB-16) to 1.70 g/cm^3 closer to shore (PCB-17a), and have a low magnetic susceptibility ranging from 10 to 14 (SI x 10^{-5}) (Bröder et al., 2022). Grain size is dominated by fine silt (2-16 µm) at all sites (Fig. 4) followed by clay at the Mackenzie Trough sites (PCB-16, PCB-17 and PCB-18), and coarser silt and sand at PCB-17a. Downcore the dominance of the fine silt-fraction continues at all sites. PCB-16 and PCB-18 both show increasing clay-content downcore, from 15% at the top (both sites) to 30% at the base of PCB-16 and 25% in PCB-18. Both cores also feature occasional sand-bearing intervals. There is a clear trend of decreasing grain-size moving offshore, with the top of PCB-17a having 25% of material being 16 µm or coarser, PCB-17 at 17.5%, and PCB-16 and PCB-18 both having 10%.

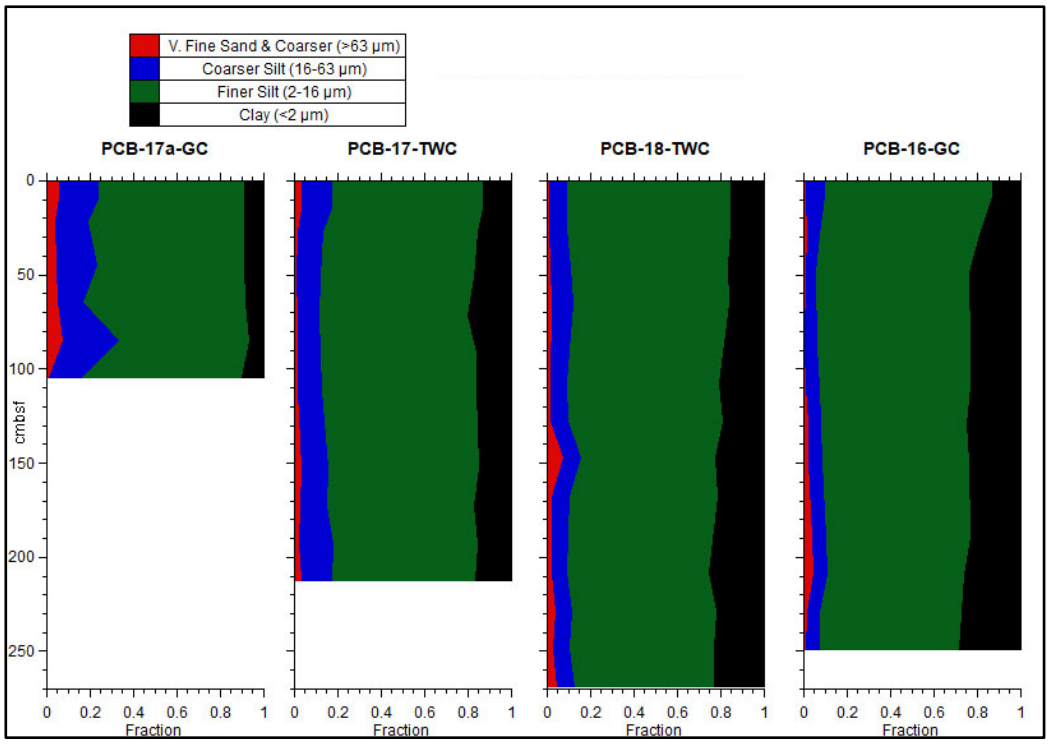

Figure 4. Measured grain size distributions from bulk syringe samples.

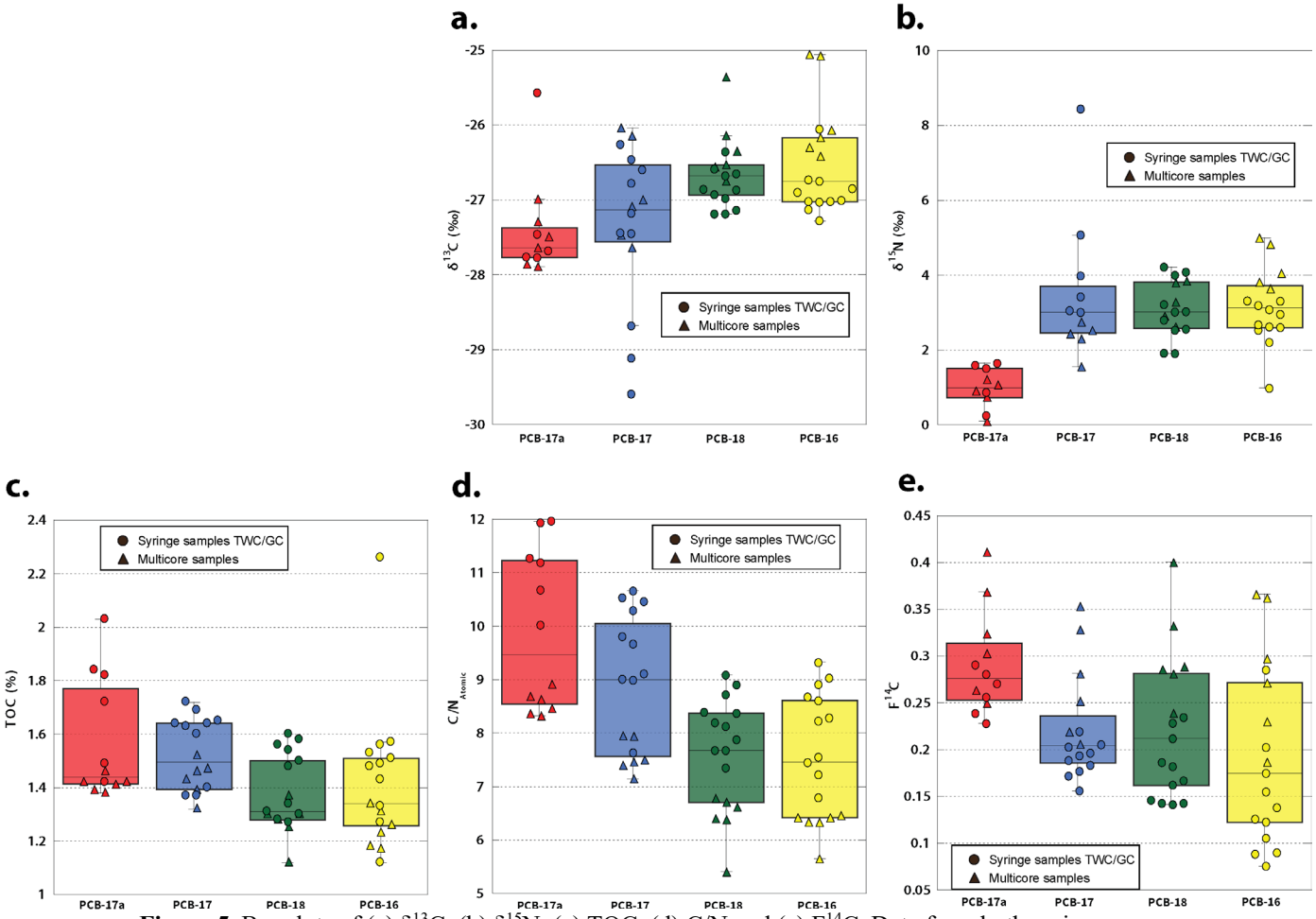

Figure 5. Boxplots of (a) $\delta^{13}C$, (b) $\delta^{15}N$, (c) TOC, (d) C/N and (e) $F^{14}C$. Data from both syringe samples and multicore samples. The line in each box is the median for both sample suites together.

Total organic carbon content decreases moving offshore, and the highest contents are found in the MUC samples at the top of the cores (Fig. 5c). The site means range from 1.37% ± 0.1% at PCB-18 to 1.56% ± 0.2% at PCB-17a. There is one notable excursion in PCB-16-GC at 8.5 cmbsf, where the carbon content is 2.3%, however, this high TOC value is not found in PCB-16-MUC where measurements were made at 5.5 and 10.5 cmbsf.

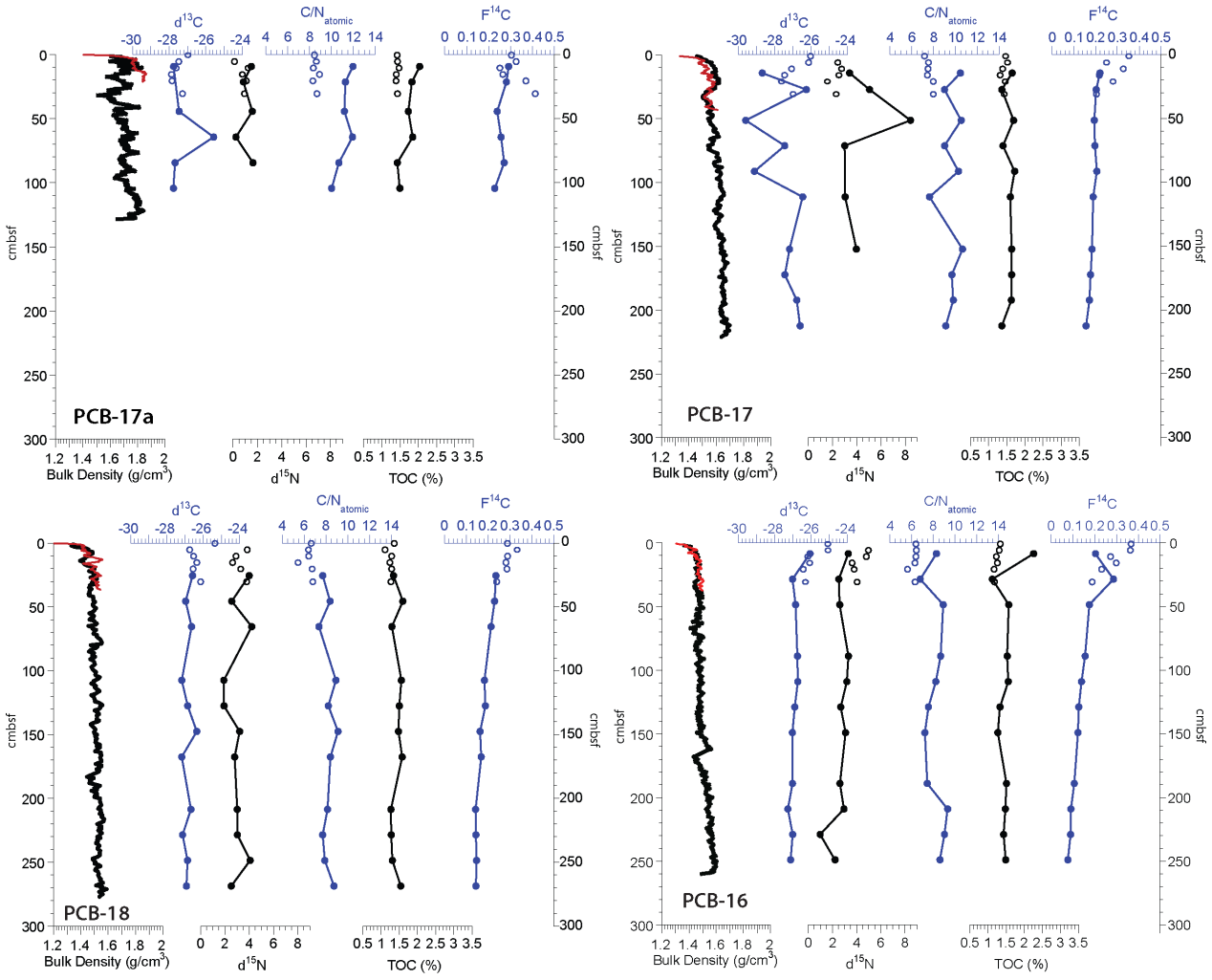

Figure 6. Downcore plots from syringe samples and MUC. Solid dots with lines and the black line for bulk density represent the syringe samples, while the empty dots and the red line for bulk density represents the MUC.

The $\delta^{13}C$ (Fig. 6) is generally highest in the near-surface MUC samples. The surface-sample (MUC 0.5 cmbsf) has the highest values at all the sites except for PCB-17a, which has an excursion at 64.5 cmbsf, reaching -25.6‰. There is a trend of increasing $\delta^{13}C$ values moving offshore (Fig. 5a), suggesting an increased input of marine OC.

PCB-16 has mean values of -26.9‰ ± 0.3‰ for syringe samples, without a clear downcore increase or decrease, and -25.9‰ ± 0.6‰ for MUC samples covering the top 30 cm. PCB-18 similarly has a stable values with a mean of -26.9‰ ± 0.3‰ in the downcore syringe samples, and -26.3‰ ± 0.5‰ for MUC samples. PCB-17 has significantly more variability with several very low outliers near the top of the core, stabilizing between -27‰ and -26‰ at 111.5 cmbsf and below. The resulting mean is -27.6‰ ± 1.2‰ for syringe samples and -26.9‰ ± 0.7‰ for MUC. PCB-17a has a mean of -27.2‰ ± 0.9‰ in the syringe samples, and -27.5‰ ± 0.3‰ for MUC.

The $\delta^{15}N$ of organic matter is stable between PCB-17, PCB-18 and PCB-16, with site means of 3.5‰ ± 1.9‰, 3.1‰ ± 0.7‰ and 3.2‰ ± 1.0‰ respectively (Fig. 5b). The shallowest site (PCB-17a) has notably lower values, with a mean of 1.0‰ ± 0.5‰ indicative of higher input of terrestrial POC versus marine POC. There is no clear downcore trend, but PCB-17 has one very high measurement of 8.4‰ at 51.5 cmbsf.

The C/N ratios show a clear decreasing trend moving offshore consistent with a decreased input of terrestrial OC, as well as a clear increase downcore at all sites, especially visible when comparing the top of the cores (MUC samples) with the longer cores (syringe samples) (Fig. 5d). PCB-17a has a mean of 11.2 ± 0.7 for the syringe samples, but only 8.6 ± 0.2 for the shallower MUC samples. PCB-17 has a syringe sample mean of 9.6 ± 0.9 and 7.6 ± 0.3 for MUC. For PCB-18, the syringe sample mean is 8.2 ± 0.5 and for the MUC it's 6.4 ± 0.5. Lastly, PCB-16 has a syringe sample mean of 8.2 ± 0.8 and a MUC mean of 6.3 ± 0.3.

$F^{14}C$ generally decreases downcore, which is expected as the sediments get older. Near the top of PCB-16-GC there is one outlier with a high $F^{14}C$ (i.e. younger age) at 28.5 cmbsf that is not captured in the MUC. PCB-17-MUC displays considerable downcore variation in age of the OC, similar to the variations seen in other bulk organic measurements at this site, while PCB-17a-MUC generally increases downcore.

3.2 Correlation analysis

A correlation analysis was performed between the elemental, grain size, and organic measurements (Fig. 7). There are two clear groupings that emerge, one associated with the silt-fraction and the other with the clay-fraction. TOC and C/N ratio are both positively correlated with the silt-fraction, and negatively correlated to clay, the C/N ratio with a R value of -0.6. The $F^{14}C$ has a strong positive correlation to silt (R = 0.85) while having negative correlation to clay, suggesting that older carbon is associated with the silt-sized fraction. Isotopes of C and N show very little correlation to the other parameters. $\delta^{13}C$ has a weak positive correlation (R = 0.25 to 0.45) to some of the elements within the group that is positively correlated with clay. Ca, which is in the silt-grouping, has strong negative correlation to all elements within the clay-grouping. Al, Fe and K all show strong positive correlation to elements within the clay group, and strong (R = -0.8 to -1) negative correlation to the C/N ratio and to Ca. Ti has no significant correlation to either clay or silt and is very weakly positively correlated (R = 0.3 to 0.4) to elements in the clay-group, and to the Al/TOC ratio. The AL/TOC was included in the analysis as it was used as a means of quantifying the petrogenic POC contribution to samples in the Mackenzie River by Hilton et al. (2015). Similarly, the Si/Ti ratio was included since it was used by Hilton et al. (2015) as a proxy for grain size. The silt/clay ratio was included as an additional grain-size parameter.

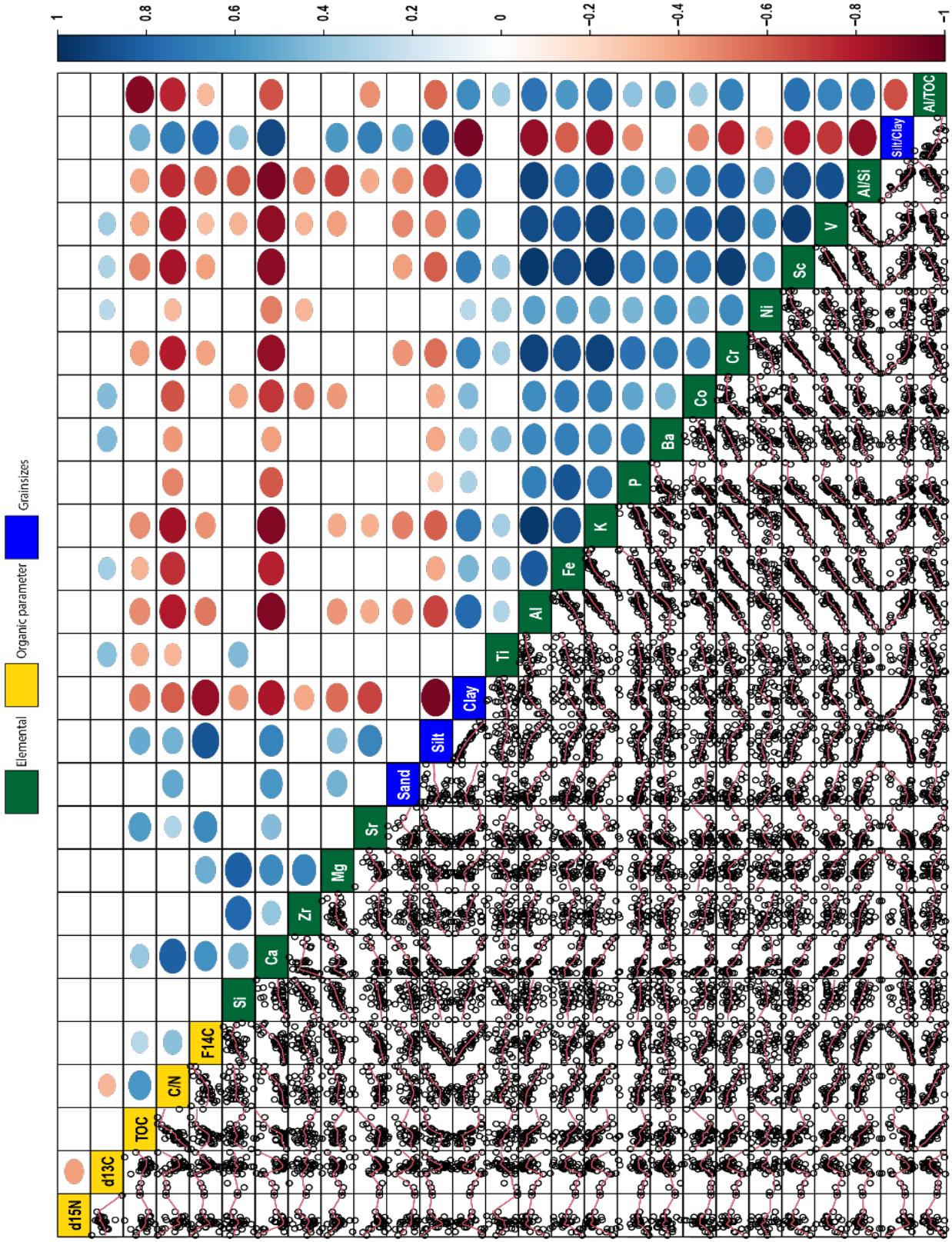

Figure 7. Results from the correlation analysis shown as both crossplots and by dots, coloured and sized depending on the R-value. Elemental data without any significant correlation are omitted from the figure.

3.3 OC burial rates

The mass accumulation rate (MAR) of OC (MAR_{OC}) is derived from a simple linear equation realting the sedimentation rate (SAR), the dry density and TOC content. It is calculated by multiplying the SAR aquired from the radioisotope data with the average dry density (ρ_d) and the fraction of OC (0-1).

(5) $$MAR_{OC}\ (g\ cm^{-2}yr^{-1}) = SAR\ (cm\ yr^{-1} * \rho_d(g\ cm^{-3}) * OC$$

Sedimentation rates were derived from radioisotope measurements (Figure 8 and Table 3). PCB-17a did not show any detectable ^{137}Cs extinction, and the ^{210}Pb data did not display a smooth downcore decay profile. As a result, no SAR could be calculated for this site. However, since PCB-17a is located outside the Mackenzie Trough, it is not needed to calculate the OC burial rate. Further radioisotope dating of the longer gravity core from this site is being conducted to improve the age modelling. Basal ages for the analyzed cores are presented in Table 3. Overall, lower SAR and older basal ages are found further offshore.

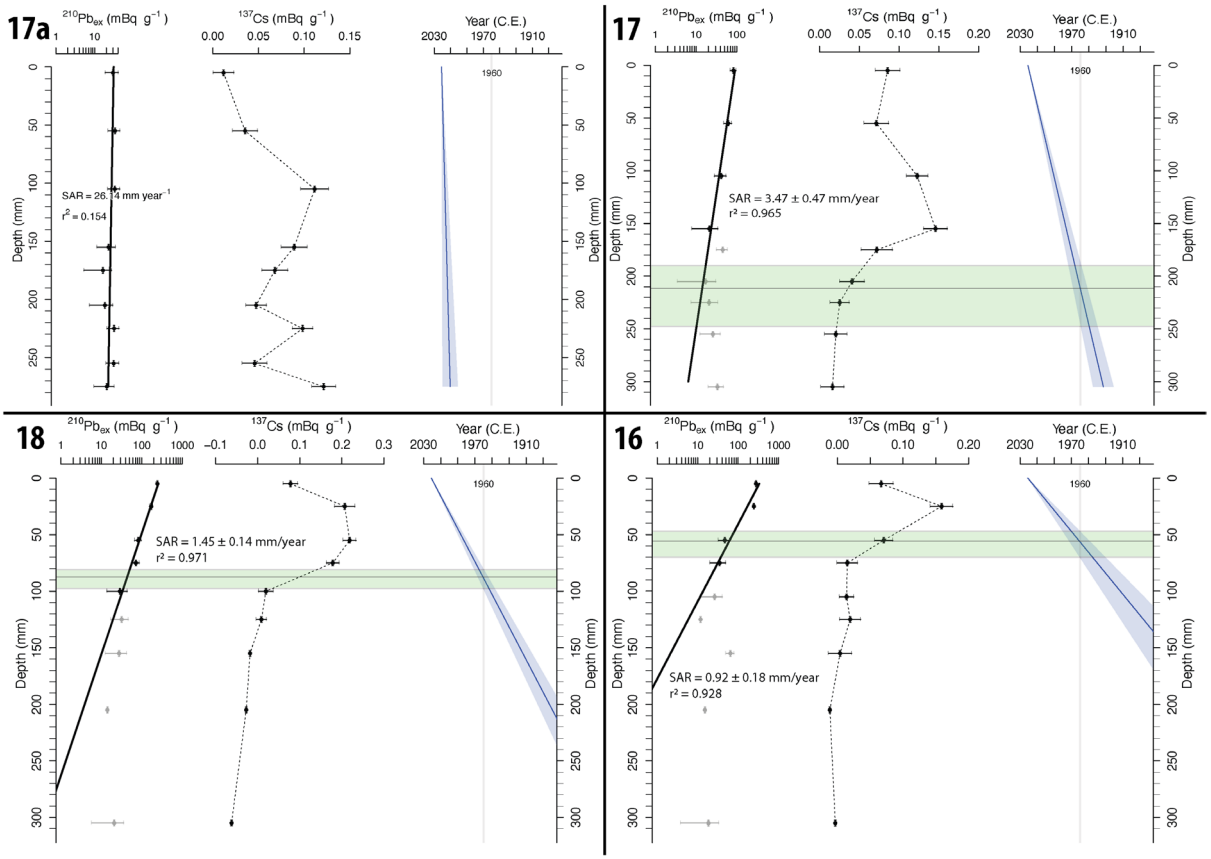

Figure 8. Results from the radioisotope measurements and age modelling. Grey points are omitted from the calculation of the SAR. Blue field indicates the age resulting from the model. Green field indicates the depth of the year 1960 (line), with associated standard deviation (width of green field).

Site	SAR (cm/year)	Max core depth (cm)	Extrapolated basal age (cal. yr BP)
PCB-17-TWC	0.347 ± 0.047	232.5	599 ± 92
PCB-18-TWC	0.145 ± 0.014	288.5	1919 ± 170
PCB-16-GC	0.092 ± 0.018	269	2853 ± 595

Table 3. Sediment accumulation rates, core depths and extrapolated basal ages for cores in the Mackenzie Trough.

In order to calculate the amount of sediment deposited in the trough, the dry density of the sediments are required. It is defined as:

(6) $$\rho_d = \frac{Mass\ of\ solids}{Volume\ of\ solids + pore\ space}.$$

The bulk density (ρ_b) for each core was aquired from the shipboard MSCL mesurements. An average value for the upper 10 cm was used for PCB-17, PCB-18 and PCB-16. For saturated marine sediments, the bulk density can be used to calculate the dry density:

(7) $$\rho_d = \left(\frac{\rho_b - \rho_w}{S_G - 1}\right) * S_G$$

where ρ_w is the density of pore-water ($1.024\ g/cm^3$) and S_G is the specific gravity of the sediment, calculated by dividing the grain density (ρ_G) by the density of water (ρ_w):

(8) $$S_G = \frac{\rho_G}{\rho_w}$$

The average grain density (ρ_G) of the syringe samples were measured on a pycnometer, and an average for each site was calculated (Table 4).

Site	Grain density (g/cm^3)	Specific gravity (g/cm^3)	Bulk density (g/cm^3)	Dry density (g/cm^3)
PCB-17	2.68 ± 0.010 (n = 5)	2.62	1.46	0.70
PCB-18	2.67 ± 0.002 (n = 6)	2.61	1.37	0.56
PCB-16	2.69 ± 0.018 (n = 8)	2.63	1.38	0.57

Table 4. Average grain density, specific gravity, bulk density and dry density for cores in the Mackenzie Trough.

The mass accumulation rate (Table 5) was calculated by multiplying the SAR from the radioisotope data with the average dry density:

(9) $$MAR\ (g\ cm^{-2}\ yr^{-1}) = SAR\ (cm\ yr^{-1}) * Dry\ density\ (g\ cm^{-3}).$$

Site	PCB-17	PCB-18	PCB-16
MAR (g cm^{-2} yr^{-1})	0.243 ± 0.033	0.081 ± 0.008	0.052 ± 0.010
Average OC content (%)(Whole core)	1.57	1.43	1.50
Organic carbon content (%) (Surface sample)	1.65	1.34	2.26
MAR$_{OC}$ (whole core %OC) (g m^{-2} yr^{-1})	38 ± 5	11 ± 1	8 ± 1
MAR$_{OC}$ (Surface sample %OC) (g m^{-2} yr^{-1})	40 ± 5	11 ± 1	12 ± 2

Table 5. Mass accumulation rates, TOC values and OC burial rates for cores in the Mackenzie Trough.

These MARs of OC are broadly consistent with those reported by Macdonald et al (1998) that were derived using the thickness of post-transgression sediments across the shelf and delta. The MAR_{OC} for PCB-17 (40 ± 5 g m^{-2} yr^{-1}) is certainly higher than what is reported for the areas just landward of the Mackenzie Trough (i.e. <50 m water depth) in Macdonald's budget (5-15 g m^{-2} yr^{-1}), but is consistent with arguments for high sediment accumulation in the Mackenzie Trough (Harper and Penland, 1982; Macdonald et al., 1998). The MAR_{OC} decreases offshore, and the general pattern and magnitudes are rather consistent with those reported by Macdonald et al. (1998) who estimate OC burial rates of 65 – 156 g m^{-2} yr^{-1} near the mouth of Mackenzie River, decreasing to 0-6 g m^{-2} yr^{-1} on the outer shelf, with the lowest MARs found on the eastern shelf far from the Mackenzie River and Mackenzie Trough.

3.4 Source Partitioning

To identify the source of the OC in the Mackenzie Trough, 4 endmember models were run. Two relied solely on $\delta^{13}C$ with two endmembers being defined (Marine vs. Terrestrial; Marine vs Mackenzie River POC), and two used $\delta^{13}C$ and $F^{14}C$ with 3 endmembers (Table 6).

	Endmember 1	**Endmember 2**	**Endmember 3**
Model 1	Marine[a] $\delta^{13}C$: -20.2‰ ± 1.7‰	River POC[b] $\delta^{13}C$: 27.4‰ ± 0.5‰	Not used
Model 2	Marine[a] $\delta^{13}C$: -20.2‰ ± 1.7‰	Shallow soil[b] $\delta^{13}C$: -27.8‰ ± 1.7‰	Not used
Model 3	Marine[a] $\delta^{13}C$: -20.2‰ ± 1.7‰ $\Delta^{14}C$: 0	Shallow soil[b] $\delta^{13}C$: -27.8‰ ± 1.7‰ $\Delta^{14}C$: -228.3‰ ± 211.2‰	Petrogenic[b] $\delta^{13}C$: -24.4‰ ± 2.4‰ $\Delta^{14}C$: -1000
Model 4	Marine[a] $\delta^{13}C$: -20.2‰ ± 1.7‰ $\Delta^{14}C$: 0	Shallow soil[b] $\delta^{13}C$: -27.8‰ ± 1.7‰ $\Delta^{14}C$: -228.3‰ ± 211.2‰	Petrogenic[a] $\delta^{13}C$: -27.6‰ ± 2.7‰ $\Delta^{14}C$: -1000

Table 6. Endmembers used in models, and their associated values. Endmembers taken from [a]Kim et al. (2022) and [b]Behnke et al. (2023).

Endmembers for the 2-endmember models were chosen based on the assumption that shelf OC should primarily come from two sources, marine primary production and a terrestrial source. In Model 1, shallow soils were chosen as the terrestrial endmember as its composition is well defined in Behnke et al. (2023) and is based on 130 $\delta^{13}C$ measurements. It is also the endmember having a $\delta^{13}C$ range wide enough to encompass the range of values found in our dataset (Fig. 1). These results were compared with Model 2, where the Mackenzie River POC endmember was used instead of the shallow soils endmember. The $\delta^{13}C$ range of the PCB samples mostly overlap with this endmember. Additionally, its use is justified by the argument that most terrestrial carbon that enters the shelf is transported by Mackenzie River, making this endmember a logical choice for a marine/terrestrial modelling.

The results of the 2-endmember models show a low contribution from marine primary productivity (PP) (Fig. 9). When modelled against Mackenzie River POC, the marine fraction constitutes on average 7% ± 4% of OC at PCB-17a, increasing further offshore to 14% ± 7% for PCB-16. Modelling marine PP against the shallow soils yields higher average fractions of marine PP, ranging from 18% ± 11% at PCB-17a, again increasing further offshore to 24% ± 13% at PCB-16. In short, there is a 6%-7% difference in the proportion of the marine and terrestrial OC sources predicted by these two models.

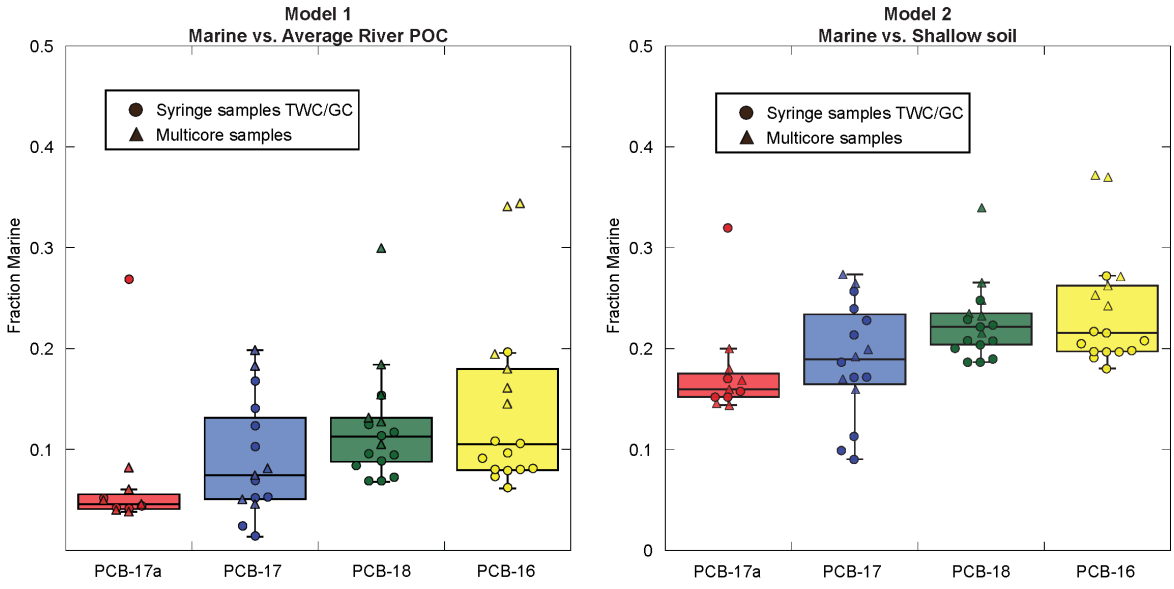

Figure 9. Results of the two 2-endmember models. The marine fraction is displayed on the Y-axis, the second fraction can be calculated by (1 – marine fraction).

Figure 1 illustrates that there is a need to include a petrogenic endmember, as the PCB samples have a much lower $F^{14}C$ value than the terrestrial and marine endmembers. Model 3 and Model 4 are 3-endmember models that employ the marine endmember (Kim et al., 2022), the shallow soil endmember (Behnke et al., 2023) and two different petrogenic endmembers, one from Kim et al. (2022) and the other from Behnke et al. (2023) (Table 6).

The results from the 3-endmember models indicate that petrogenic carbon constitutes the vast majority of OC in our samples with site averages ranging from 56% to 66% in model 3, and from 60% to 70% in model 4 (Fig. 10). Shallow soils are the second largest source of OC, followed by marine primary production. While PCB-17a and PCB-17 do not display any clear downcore trend, both PCB-18 and PCB-16 show a downcore decrease in the petrogenic fraction. This is balanced by an increase in the soil fraction, which can be seen to increase with depth.

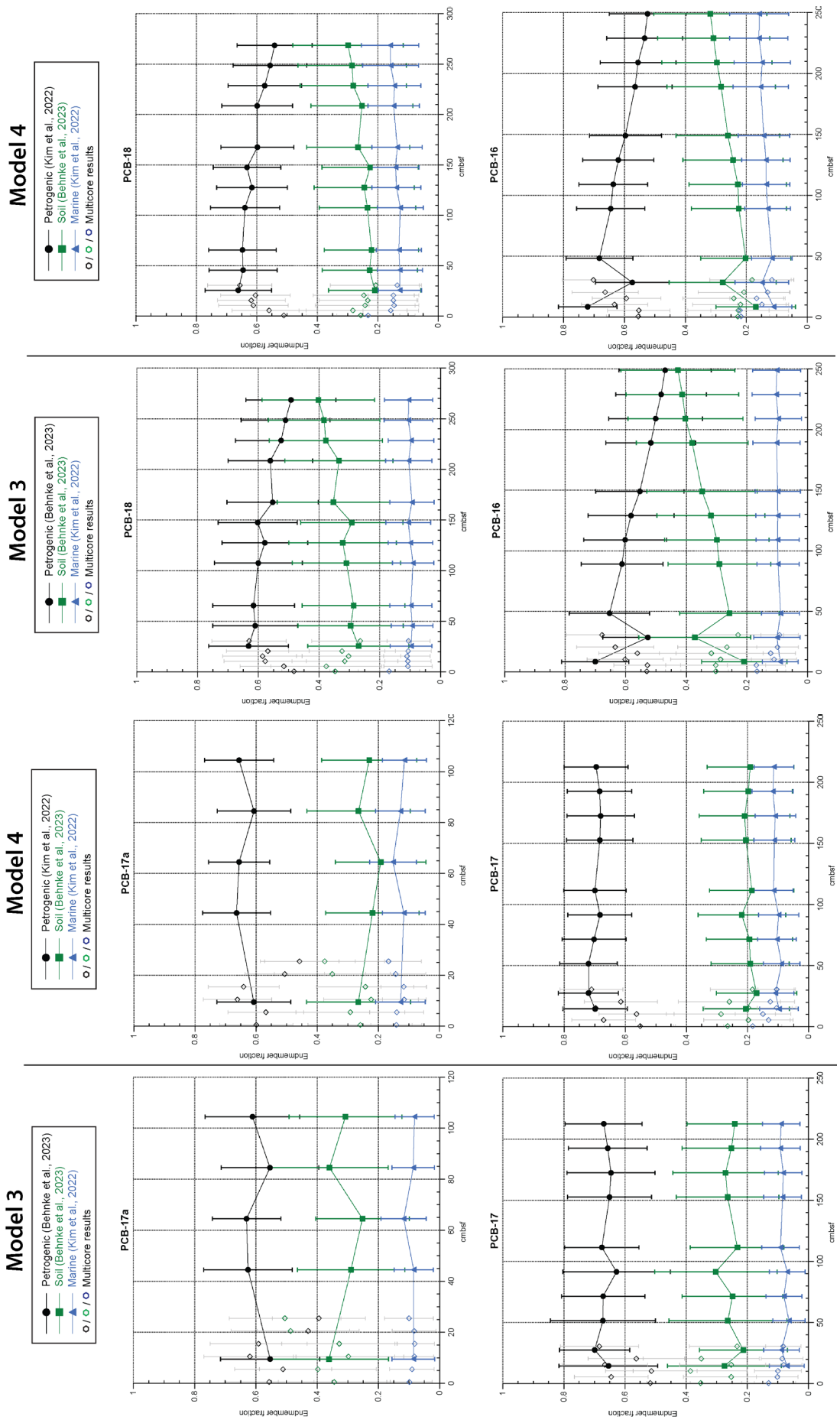

Figure 10. Results of the 3-endmember models.

4.0 Discussion

4.1 Carbon Burial in the Mackenzie Trough

Estimating the total burial of terrestrial POC in the Mackenzie Trough is one of the primary objectives of this study. The total area of the trough, as defined in this study, is 9152 km^2. A basic estimate of the MAR$_{OC}$ in the trough is found from the average of PCB-17, 18, 16:

$$MAR_{avg.} = \frac{MAR_{PCB-17} + MAR_{PCB-18} + MAR_{PCB-16}}{3}$$

$$= \frac{0.243 \pm 0.033\ g\ cm^{-2}\ yr^{-1} + 0.081 \pm 0.008\ g\ cm^{-2}\ yr^{-1} + 0.052 \pm 0.010\ g\ cm^{-2}\ yr^{-1}}{3}$$

$$= \frac{0.376 \pm 0.051}{3} = 0.125 \pm 0.017\ g\ cm^{-2}\ yr^{-1}$$

The average MAR is multiplied by the area of Mackenzie Trough, and converted to Millions of tonnes (Mt):

$$MAR_{MT} = MAR_{avg.} * Area_{MT} = 0.125 \pm 0.017\ g\ cm^{-2}\ yr^{-1} * \ 9152\ km^2$$
$$= 0.125 \pm 0.012\ g\ cm^{-2}\ yr^{-1} * (9152\ km^2 * 10^{10})\ cm^2$$
$$= 1.144 * 10^{13} \pm 1.098 * 10^{12}\ g/yr = 11.44 \pm 1.098\ Mt/yr$$

From here, two approaches are taken to determine the MAR$_{OC}$. The annual carbon burial is calculated using both the average carbon content of all syringe samples, as well as the average TOC of the MUC samples, to obtain a more accurate estimate of modern carbon burial. The TOC values used are presented in Table 7.

Site	PCB-17	PCB-18	PCB-16	Average
Ave. syringe sample OC (%)	1.57 ± 0.1	1.43 ± 0.1	1.50 ± 0.3	1.50 ± 0.1
Ave. MUC OC (%)	1.43 ± 0.1	1.27 ± 0.1	1.24 ± 0.1	1.31 ± 0.1

Table 7. TOC values used for calculating the annual carbon burial.

$$Annual\ carbon\ burial\ (Syringe\ sample\ TOC) = MAR_{MT} * TOC$$
$$= 11.44 \pm 1.098\, Mt/yr * (0.015 \pm 0.001) = 0.17 \pm 0.02\ Mt\ Carbon/yr$$

$$Annual\ carbon\ burial\ (MUC\ sample\ TOC) = MAR_{MT} * TOC$$
$$= 11.44 \pm 1.098\, Mt/yr * (0.0131 \pm 0.001) = 0.15 \pm 0.02\ Mt\ Carbon/yr$$

The results show that both approaches provide similar estimates for OC burial rates. The modern estimate of 0.15 ± 0.02 Mt C/yr can be compared to the carbon budget presented by Macdonald et al. (1998). They estimated that 0.71 ± 0.3 Mt C/yr was buried on the Beaufort Shelf, this is approximately 4.7x more than what is buried in the Mackenzie Trough. However, the shelf has an area of 60,000 km^2, more than 6x that of Mackenzie Trough. Adding our estimate for burial in the Mackenzie Trough to the Macdonald et al. (1998) budget would account for almost all the OC they estimate to be lost at the shelf edge (0.17 ± 0.2 Mt C/yr). Compared to the total input of POC carried by the Mackenzie River (2.1 Mt/yr, Fig. 2), the Mackenzie Trough accounts for about 7% of this POC, bringing the total percentage of river derived POC accounted for in delta- and shelf sediments up to 87% (when using Macdonald et al.'s value without post-sedimentation oxidation). When comparing to the annual input of POC to the shelf (i.e. that is estimated to bypass the delta), of the 1.21 Mt that escapes the delta 12.4% is buried in the Mackenzie Trough.

Putting these results of into context of the 46% increase in sediment load, and 22% increase in Mackenzie River output reported in Doxaran et al. (2015), there is no clear evidence of a recent increase in carbon burial rates in Mackenzie Trough. However, the satellite-based sediment load observations of Doxaran et al. (2015) were smaller than those used by Macdonald et al. (1998) by at least a factor of 2. This would imply that POC burial in the delta, shelf and Mackenzie Trough is in larger than the POC delivered by Mackenzie River each year. However, there are a number of overlooked, or poorly estimated sources/sinks that could account for this discrepancy. This includes a poorly constrained input of terrestrial OC from coastal erosion, and poorly constrained burial estimates in the modern delta, which accounts for the largest sink of terrestrial OC delivered by the Mackenzie River.

4.2 Sources of OC in the Mackenzie Trough

The results of the 2-endmember model (Fig. 9) reveal a clear trend of increasing marine input moving offshore. Supporting this, the C/N ratio also decreases offshore (Fig. 5d). This is interpreted to reflect a lower input of terrestrial OC, which generally has a higher C/N (>20), when compared to marine PP (~7) (Behnke et al., 2023; Goñi et al., 2005; Kim et al., 2022).

Hilton et al. (2015) used a combination of a 2-endmember cross plot between $\delta^{13}C$ and N/OC, together with the Al/OC ratio to support his conclusion that all the terrestrial POC delivered by the Mackenzie River is buried offshore. The coring-site in their study (MTW01) is in close proximity to PCB-17, in Mackenzie Trough. The same approach was attempted in this study, but the data from PCB-17 does not fall between the two endmembers used by Hilton et al. (2015) (Fig. 1), with the PCB samples having a higher N/OC ratio and more negative $\delta^{13}C$ signature than the MTW01 samples. Furthermore, they use Al to normalize the TOC content of the core with the goal of removing effects from dilution (increased/decreased sediment input with constant OC influx). The correlation analysis of the PCB measurements (Fig. 7) reveals that the Al/TOC ratio is positively correlated (R = 0.6) to clay, and negatively correlated (R = 0.5) to silt. The Al itself is also correlated positively to clay (R = 0.8) and negatively to silt (R = 0.5). One explanation is that the Al/OC ratio is impacted by grain size (transport processes) rather than sedimentation rates. We should also consider

the strong correlation between silt and OC, and the fact that all our sites are dominated by silt, further reducing the viability of Al as a normalizing factor regarding dilution of OC in the sediment.

Results from the 3-endmember models highlight the fact that OC in the Mackenzie Trough is dominated by petrogenic carbon. This finding is consistent with previous studies, which also found the petrogenic fraction to be dominant on the Beaufort Shelf (Goñi et al., 2005; Kim et al., 2022), and in deglacial and Holocene sediments from the Beaufort Sea Slope (Wu et al., 2022). When comparing the marine fractions between the different end member models (Fig. 11), the 3-EMM models do not display the offshore increase as clearly as the 2-EMM models do, but have more consistent marine fraction between the sites (Fig. 12). In fact, the largest difference in estimates for marine PP inputs come from Model 2, whereas Models 1, 3 and 4 provide broadly consistent (overlapping) results.

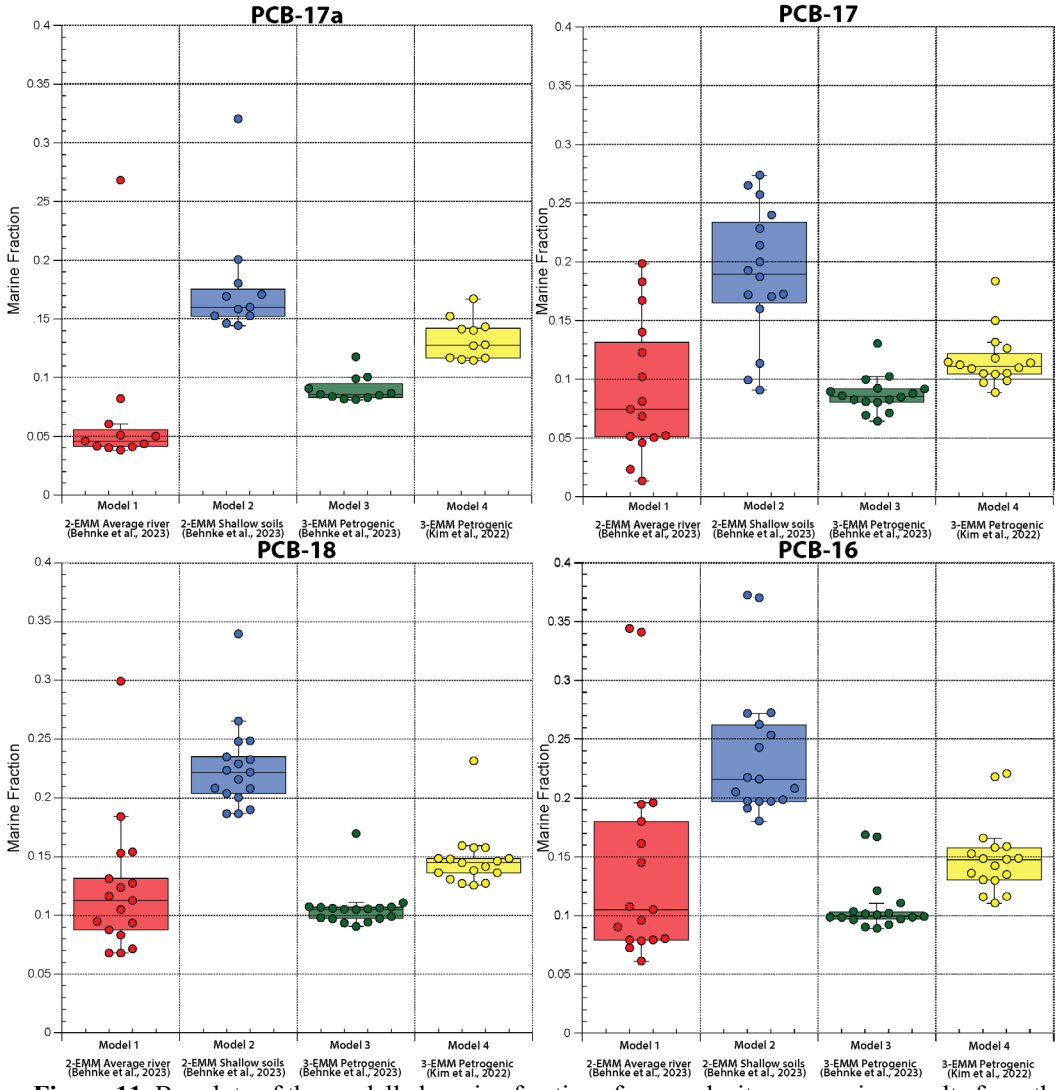

Figure 11. Boxplots of the modelled marine fractions from each site, comparing results from the different models. The line in each box represents the median value.

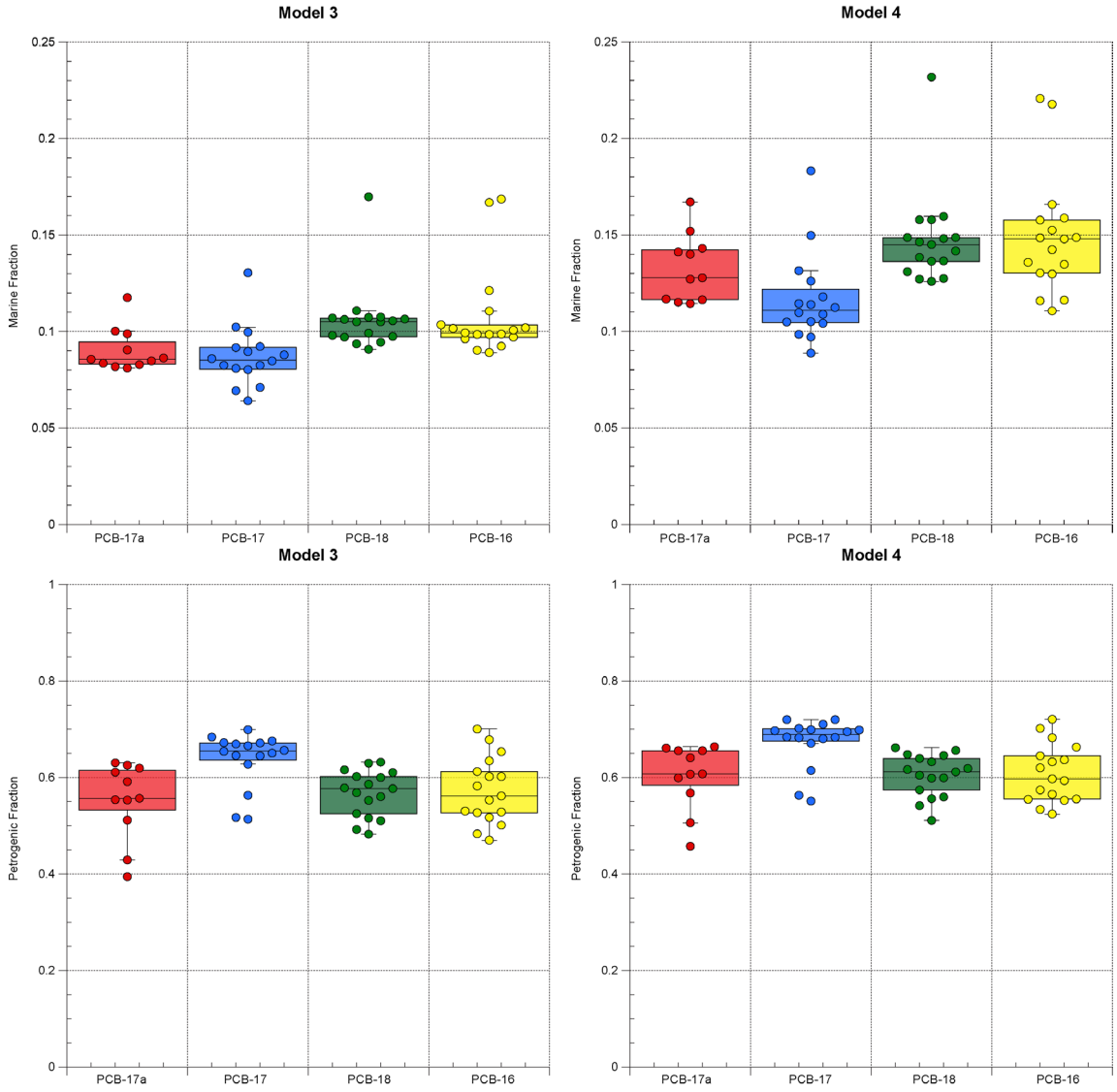

Figure 12. Boxplots displaying the offshore (sitewise) trends for the marine and petrogenic fractions. The line in each box represents the median value.

4.3 Downcore variation in OC sources

The apparent decrease in petrogenic OC downcore that is found in the 3-endmember models for PCB-18 and PCB-16 (Fig. 10) is interesting. When constructing these models, the $\Delta\Delta^{14}C$ is calculated for the age. This should give the age difference between the organic carbon and the depositional age, or in other words, the age of the OC at the time of deposition. This method attempts to get rid of any signal from the age increase that naturally comes with increasing depth in the core. However, in PCB-18 and PCB16, there is an increase in $\Delta\Delta^{14}C$ moving downcore, suggesting that the age of OC being deposited in the sediments is decreasing downcore.

The question is if this is a real signal or if it is the result of poor age estimates arising from the linear extrapolation of sedimentation rates derived from radioisotope dating. In future studies, the integration of the radioisotope chronologies with 14C data from microfossils will allow this to be determined. Here the impact of a poor radioisotope age model is illustrated using a basic sensitivity test under the assumption that our ^{210}Pb age model is overestimating the depositional age of our samples (i.e. underestimating the SAR). Taking the deepest syringe sample from PCB-18 ($F^{14}C$ = 0.143, $\Delta^{14}C$ = -858‰, $\delta^{13}C$ = -26.93) with an estimated age of deposition of 1785 cal. yr. bp, equations (1) and (2) are combined into equation (10) where the modelled age is used to calculate an expected $\Delta^{14}C$ value which is then subtracted from the measured $\Delta^{14}C$ of the sample, yielding the $\Delta\Delta^{14}C$.

$$\Delta^{14}C = \left(e^{\frac{Modelled\ age}{-8033}} - 1\right) * 1000 \quad (10)$$

The modelled age then has the age-error added (100, 1000, 2000 and 3000 years), yielding erroneous $\Delta\Delta^{14}C$ values which are plotted together with the actual $\Delta\Delta^{14}C$ to illustrate its potential effect on source-appointment.

This exercise illustrates the sensitivity of the $\Delta\Delta^{14}C$ calculations to age-model errors and how this impacts the results in the end-member modelling space (Fig. 13). An error of 100 years and 1000 years yields a difference of 10‰ and 93‰ respectively to the resulting $\Delta\Delta^{14}C$ or the $F^{14}C$ value at the time of deposition. The 100-year error is not so dramatic as it is similar to the standard deviation of the $\Delta^{14}C$ measurements (about ±3‰), and within the standard deviation of the ^{210}Pb-based age model for this sample (±168 years). An error ≥1000 years would

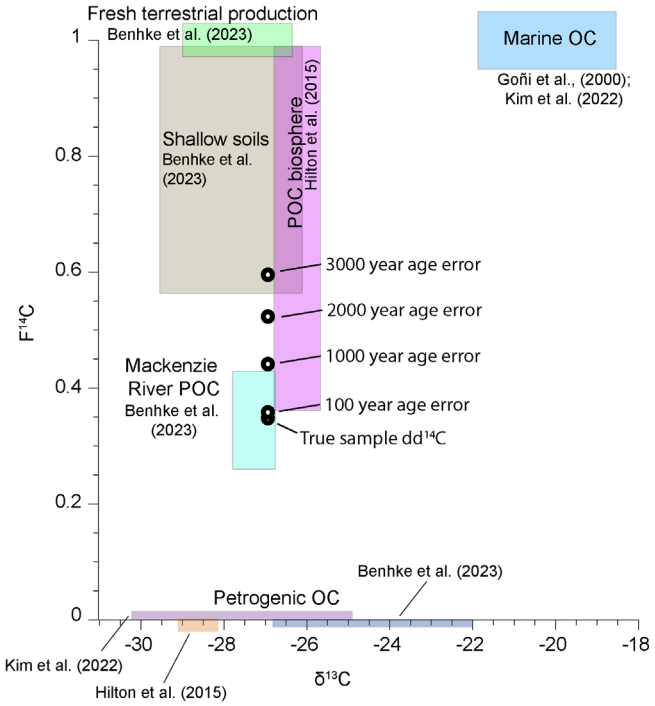

Figure 13. Result of the sensitivity test, the calculated resulting values marked as black dots overlain the endmembers identified in literature for the Mackenzie Shelf.

significantly influence the resulting modelling, leading to either a large increase in the petrogenic fraction or shallow soil and marine fractions depending on whether the age model underestimates or overestimates the true depositional age. At the two deepest sites (PCB18, PCB16), endmember modelling suggests that the petrogenic fraction decreases downcore. This could be explained by an overestimation of the true depositional age of the sample, decreasing the difference between the depositional age and the measured $F^{14}C$ of the sample, leading to younger (less negative) $\Delta\Delta^{14}C$ values. To further untangle the true nature of the increasing petrogenic fraction downcore, the age model needs to be better constrained. Solidifying the age model by picking and dating foraminifera was planned for this study but too few foraminifera were found to date. Larger samples need to be taken to achieve these objectives.

4.4 Offshore variations in OC sources

It has been reported that there is a strong linear relationship between TOC and grainsize, specifically silt and clay (Macdonald et al., 2003). Data from the Mackenzie Trough cores does not seem to align with the trends seen in a compilation of shelf sediments from the Alaskan and Canadian Beaufort Sea where OC contents increase as the fine fraction abundance increase (Fig. 14). Even the most shallow site, PCB-17a where sediments are most coarse, falls below the predicted relationship. In general, this relationship breaks down when the fine fraction abundance increases beyond 70-80%, which characterises all the PCB sediment cores in the Mackenzie Trough.

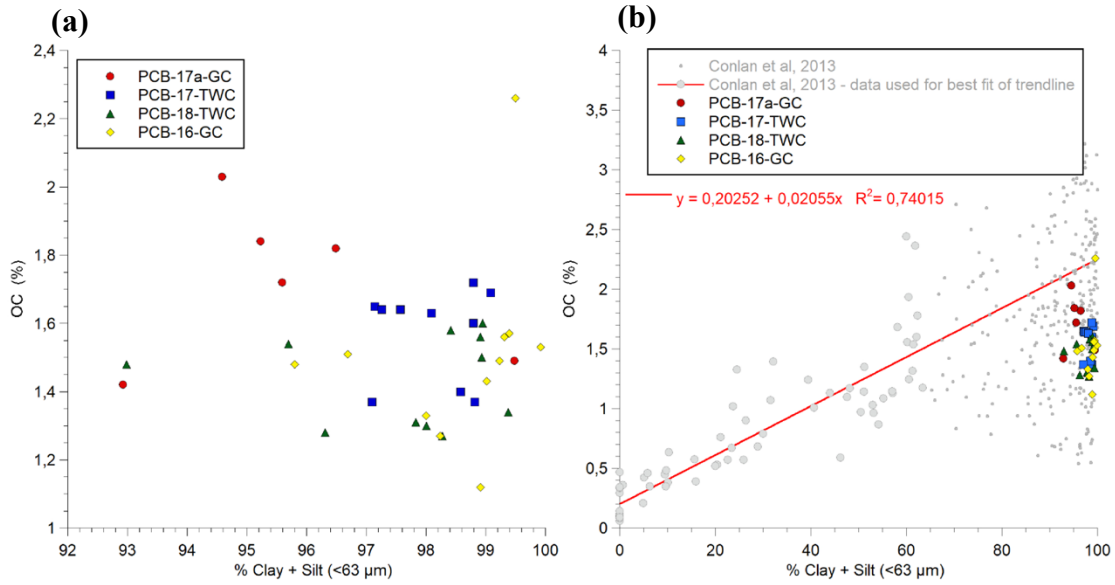

Figure 14. Plots relating the grain sizes to the organic carbon content. (a): data from this study. (b): data from Conlan et al. (2013) together with the results of this study.

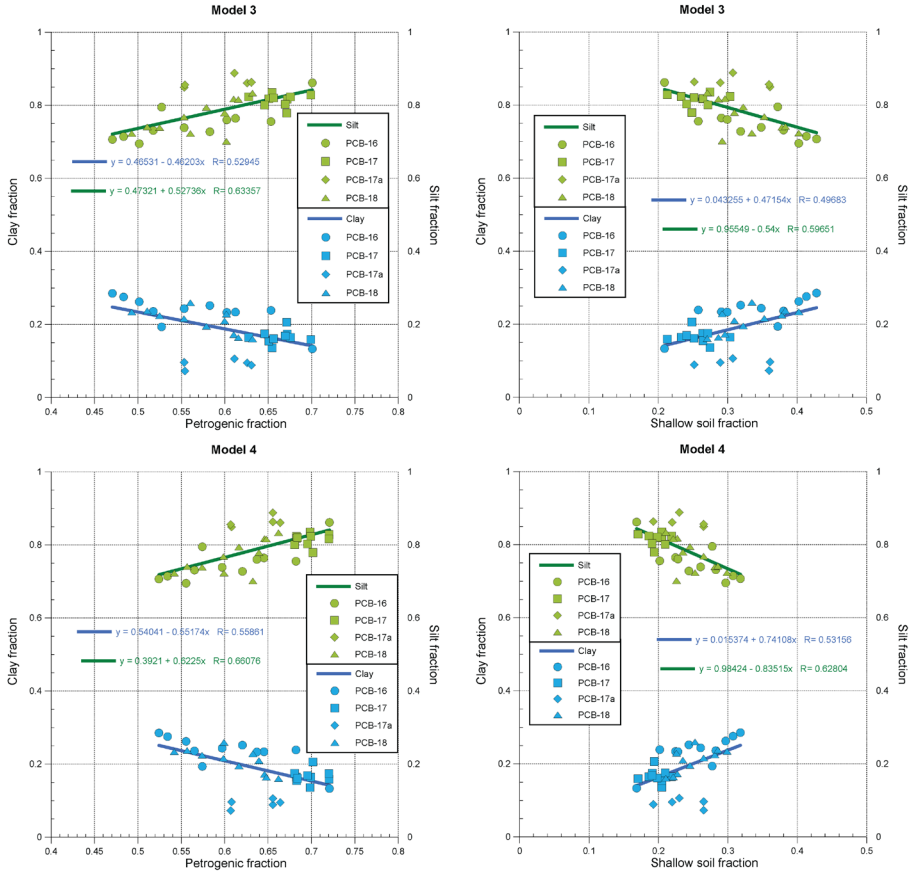

Figure 15. Correlations between the modelled petrogenic and shallow soil fractions, and silt and clay fractions.

Comparing modelled petrogenic fractions between the sites reveals that there are no clear trends when moving offshore (Fig. 12). However, PCB-17 has a notably higher fraction of petrogenic OC. To investigate this further, both terrestrial endmembers were plotted against the grain-size fractions clay and silt (Fig. 15). The shallow soil fraction correlates negatively to silt and negatively to clay. Meanwhile, the petrogenic fraction has a negative correlation to clay and a positive correlation to silt (similarly to TOC (Fig. 7)). This suggests that the petrogenic fraction is preferentially hosted in the silt fraction and highlights the potential role that sediment transport processes have on the distribution of different carbon pools offshore. This could potentially explain the downcore decrease in the petrogenic fraction, as there is an increase in the clay-fraction downcore in the deeper sites (Fig. 4). This finding is in contrast with results from (Wu et al., 2022), where they find a downcore increase in petrogenic carbon at their site ARA04C/37, further offshore and in deeper water depths than PCB-16. They attribute the increasing petrogenic fraction downcore to increased erosion and isostatic uplift during deglaciation, as well as increased sedimentation rates. However, it is important to remember that a downcore decrease in the petrogenic fraction in the PCB cores requires validation using improved age models, and constrained errors on $\Delta\Delta^{14}C$ values used in the end member modelling.

5.0 Conclusions

In this study, a modern estimate for POC burial in Mackenzie Trough (0.15 ± 0.2 Mt/yr) is presented and compared to published literature. The Mackenzie Trough was found to be a significant sink for remobilised terrestrial OC with a significant impact on the OC budget for the Beaufort Shelf, with a MAR_{OC} higher than the shelf average. Compositional and isotopic proxies have been found to reflect a lesser influence of terrestrial biogenic and petrogenic OC and increased influence from marine PP, moving offshore along the Mackenzie Trough. Endmember modelling reveals decreasing inputs of terrestrial source of OC moving offshore, but these results would require improvements to the age model to solidify the results. A downcore trend of increased input of petrogenic OC has been observed in the 3-EMM for the 2 deepest sites (PCB-18 and PCB-16), contradicting findings from previously published studies. However, these results are not concrete enough to dismiss any prior results due to the lack of a confidence in the age model it is based on. Correlational analysis has also revealed a significant preferential hosting of petrogenic POC in the silt-sized fraction of sediments. While this finding would also need to be verified with a better age model, this opens a new avenue for future research to further investigate its implications on the carbon budget for the Beaufort Shelf. The transportation and depositional environment, to name a few factors, could potentially play a big role in the fate of terrestrial carbon hailing from Mackenzie River, and future studies are encouraged to further develop this finding.

6.0 Acknowledgements

I would like to extend my deepest gratitude to my supervisor, Dr. Matt O'Regan, for always encouraging me, motivating me, supporting my work, and never giving up on me. I would also like to thank my co-supervisors Dr. Lisa Bröder and Dr. André Pellerin for their help with sampling, measurements and general advice throughout writing this thesis. Additionally, I would like to thank my parents as well as Maja, for their never-ending support, encouragement and love.

7.0 Appendix

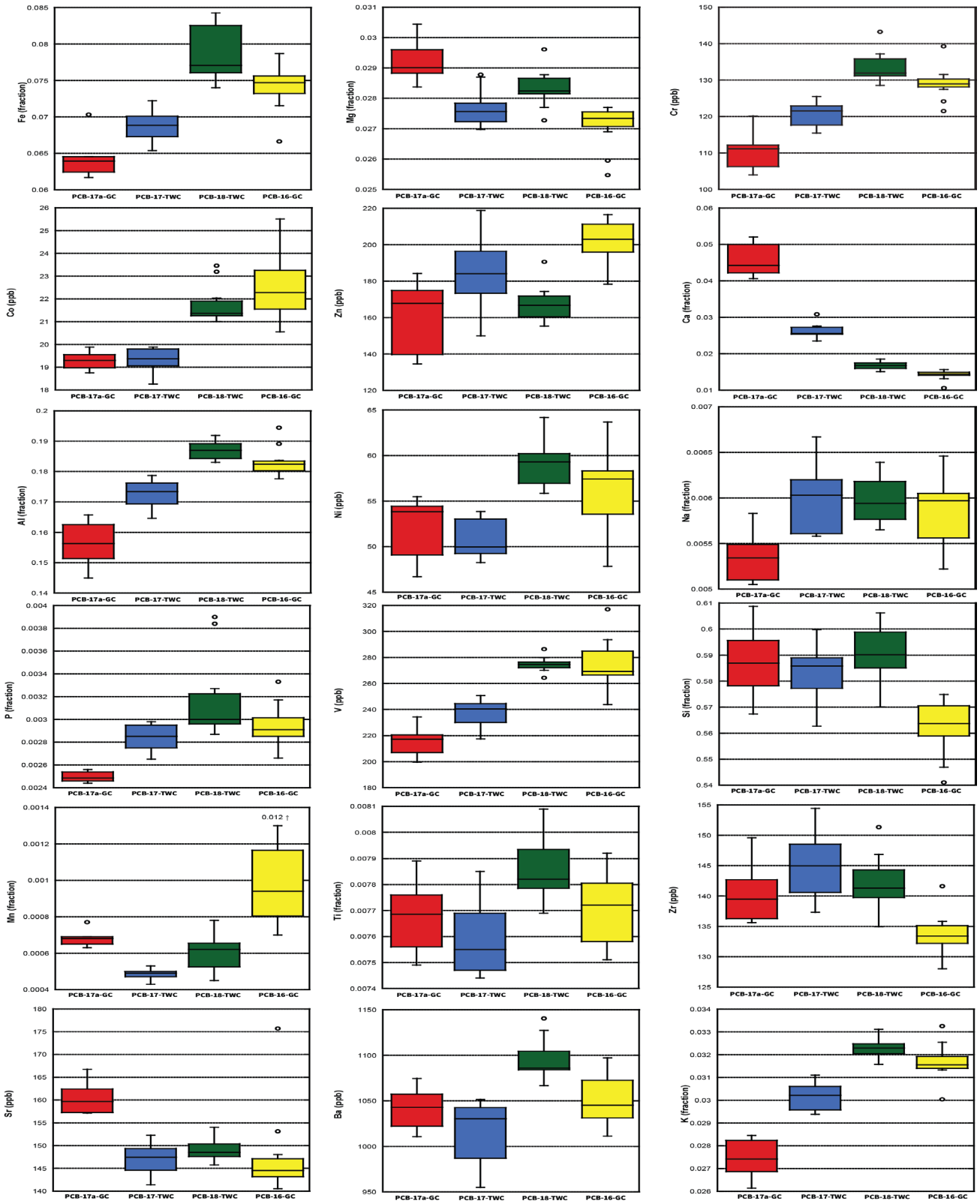

Figure A1. Boxplots of all the elemental data generated by ICP-OES. Line in each boxplot is the median value.

8.0 References

Batjes, N. h., 1996. Total carbon and nitrogen in the soils of the world. Eur. J. Soil Sci. 47, 151–163. https://doi.org/10.1111/j.1365-2389.1996.tb01386.x

Behnke, M.I., Tank, S.E., McClelland, J.W., Holmes, R.M., Haghipour, N., Eglinton, T.I., Raymond, P.A., Suslova, A., Zhulidov, A.V., Gurtovaya, T., Zimov, N., Zimov, S., Mutter, E.A., Amos, E., Spencer, R.G.M., 2023. Aquatic biomass is a major source to particulate organic matter export in large Arctic rivers. Proc. Natl. Acad. Sci. 120, e2209883120. https://doi.org/10.1073/pnas.2209883120

Blasco, S., Fortin, G., Hill, P., O'Connor, M., Brigham-Grette, J., 1990. The late Neogene and Quaternary stratigraphy of the Canadian Beaufort continental shelf.

Blott, S.J., Pye, K., 2001. GRADISTAT: a grain size distribution and statistics package for the analysis of unconsolidated sediments. Earth Surf. Process. Landf. 26, 1237–1248. https://doi.org/10.1002/esp.261

Bosch, C., Andersson, A., Kruså, M., Bandh, C., Hovorková, I., Klánová, J., Knowles, T.D.J., Pancost, R.D., Evershed, R.P., Gustafsson, Ö., 2015. Source Apportionment of Polycyclic Aromatic Hydrocarbons in Central European Soils with Compound-Specific Triple Isotopes (δ13C, Δ14C, and δ2H). Environ. Sci. Technol. 49, 7657–7665. https://doi.org/10.1021/acs.est.5b01190

Bröder, L., O'Regan, M., Fritz, M., Juhls, B., Priest, T., Lattaud, J., Whalen, D., Matsuoka, A., Pellerin, A., Bossé-Demers, T., 2022. The Permafrost Carbon in the Beaufort Sea (PeCaBeau) Expedition of the Research Vessel CCGS AMUNDSEN (AMD2104) in 2021. Berichte Zur Polar- Meeresforsch. Rep. Polar Mar. Res. 759.

Bröder, L., Tesi, T., Andersson, A., Semiletov, I., Gustafsson, Ö., 2018. Bounding cross-shelf transport time and degradation in Siberian-Arctic land-ocean carbon transfer. Nat. Commun. 9, 806. https://doi.org/10.1038/s41467-018-03192-1

Bröder, L., Tesi, T., Salvadó, J.A., Semiletov, I.P., Dudarev, O.V., Gustafsson, Ö., 2016. Fate of terrigenous organic matter across the Laptev Sea from the mouth of the Lena River to the deep sea of the Arctic interior. Biogeosciences 13, 5003–5019. https://doi.org/10.5194/bg-13-5003-2016

Bruel, R., Sabatier, P., 2020. serac: an R package for ShortlivEd RAdionuclide chronology of recent sediment cores. J. Environ. Radioact. 225, 106449. https://doi.org/10.1016/j.jenvrad.2020.106449

Campeau, A., Soerensen, A.L., Martma, T., Åkerblom, S., Zdanowicz, C., 2020. Controls on the 14C Content of Dissolved and Particulate Organic Carbon Mobilized Across the Mackenzie River

Basin, Canada. Glob. Biogeochem. Cycles 34, e2020GB006671. https://doi.org/10.1029/2020GB006671

Conlan, K., Hendrycks, E., Aitken, A., Williams, B., Blasco, S., Crawford, E., 2013. Macrofaunal biomass distribution on the Canadian Beaufort Shelf. J. Mar. Syst. 127, 76–87. https://doi.org/10.1016/j.jmarsys.2013.07.013

Dietrich, J., Dixon, J., McNeil, D., McIntyre, D., Snowdon, L., Cameron, A., 1989. The geology, biostratigraphy and organic geochemistry of the Natsek E-56 and Edlok N-56 wells, western Beaufort Sea. Geol. Surv. Can. Pap. 89, 133–157.

Doxaran, D., Devred, E., Babin, M., 2015. A 50 % increase in the mass of terrestrial particles delivered by the Mackenzie River into the Beaufort Sea (Canadian Arctic Ocean) over the last 10 years. Biogeosciences 12, 3551–3565. https://doi.org/10.5194/bg-12-3551-2015

Friedlingstein, P., Jones, M.W., O'Sullivan, M., Andrew, R.M., Bakker, D.C.E., Hauck, J., Le Quéré, C., Peters, G.P., Peters, W., Pongratz, J., Sitch, S., Canadell, J.G., Ciais, P., Jackson, R.B., Alin, S.R., Anthoni, P., Bates, N.R., Becker, M., Bellouin, N., Bopp, L., Chau, T.T.T., Chevallier, F., Chini, L.P., Cronin, M., Currie, K.I., Decharme, B., Djeutchouang, L.M., Dou, X., Evans, W., Feely, R.A., Feng, L., Gasser, T., Gilfillan, D., Gkritzalis, T., Grassi, G., Gregor, L., Gruber, N., Gürses, Ö., Harris, I., Houghton, R.A., Hurtt, G.C., Iida, Y., Ilyina, T., Luijkx, I.T., Jain, A., Jones, S.D., Kato, E., Kennedy, D., Klein Goldewijk, K., Knauer, J., Korsbakken, J.I., Körtzinger, A., Landschützer, P., Lauvset, S.K., Lefèvre, N., Lienert, S., Liu, J., Marland, G., McGuire, P.C., Melton, J.R., Munro, D.R., Nabel, J.E.M.S., Nakaoka, S.-I., Niwa, Y., Ono, T., Pierrot, D., Poulter, B., Rehder, G., Resplandy, L., Robertson, E., Rödenbeck, C., Rosan, T.M., Schwinger, J., Schwingshackl, C., Séférian, R., Sutton, A.J., Sweeney, C., Tanhua, T., Tans, P.P., Tian, H., Tilbrook, B., Tubiello, F., van der Werf, G.R., Vuichard, N., Wada, C., Wanninkhof, R., Watson, A.J., Willis, D., Wiltshire, A.J., Yuan, W., Yue, C., Yue, X., Zaehle, S., Zeng, J., 2022. Global Carbon Budget 2021. Earth Syst. Sci. Data 14, 1917–2005. https://doi.org/10.5194/essd-14-1917-2022

Goñi, M.A., Yunker, M.B., Macdonald, R.W., Eglinton, T.I., 2005. The supply and preservation of ancient and modern components of organic carbon in the Canadian Beaufort Shelf of the Arctic Ocean. Mar. Chem. 93, 53–73. https://doi.org/10.1016/j.marchem.2004.08.001

Harper, J.R., Penland, S., 1982. Beaufort Sea sediment dynamics. Woodward-Clyde Consultants.

Hilton, R.G., Galy, V., Gaillardet, J., Dellinger, M., Bryant, C., O'Regan, M., Gröcke, D.R., Coxall, H., Bouchez, J., Calmels, D., 2015. Erosion of organic carbon in the Arctic as a geological carbon dioxide sink. Nature 524, 84–87. https://doi.org/10.1038/nature14653

Hugelius, G., Strauss, J., Zubrzycki, S., Harden, J.W., Schuur, E.A.G., Grosse, G., Michaelson, G.J., Koven, C.D., O'Donnell, J.A., Elberling, B., Mishra, U., Camill, P., Yu, Z., Palmtag, J., Kuhry, P., 2014. Estimated stocks of circumpolar permafrost carbon with quantified uncertainty ranges and identified data gaps 21.

Jobbágy, E.G., Jackson, R.B., 2000. The Vertical Distribution of Soil Organic Carbon and Its Relation to Climate and Vegetation. Ecol. Appl. 10, 423–436. https://doi.org/10.1890/1051-0761(2000)010[0423:TVDOSO]2.0.CO;2

Kim, D., Kim, J.-H., Tesi, T., Kang, S., Nogarotto, A., Park, K., Lee, D.-H., Jin, Y.K., Shin, K.-H., Nam, S.-I., 2022. Changes in the burial efficiency and composition of terrestrial organic carbon along the Mackenzie Trough in the Beaufort Sea. Estuar. Coast. Shelf Sci. 275, 107997. https://doi.org/10.1016/j.ecss.2022.107997

Lantuit, H., Overduin, P.P., Couture, N., Wetterich, S., Aré, F., Atkinson, D., Brown, J., Cherkashov, G., Drozdov, D., Forbes, D.L., Graves-Gaylord, A., Grigoriev, M., Hubberten, H.-W., Jordan, J., Jorgenson, T., Ødegård, R.S., Ogorodov, S., Pollard, W.H., Rachold, V., Sedenko, S., Solomon, S., Steenhuisen, F., Streletskaya, I., Vasiliev, A., 2012. The Arctic Coastal Dynamics Database: A New Classification Scheme and Statistics on Arctic Permafrost Coastlines. Estuaries Coasts 35, 383–400.

Macdonald, R., Naidu, A., Yunker, M., Gobeil, C., 2003. The Beaufort Sea: Distribution, sources, variability and burial of carbon. Arct. Ocean Org. Carbon Cycle Present Past Berl. N. Y. Springer Publ. Co. 177–193.

Macdonald, R.W., Solomon, S.M., Cranston, R.E., Welch, H.E., Yunker, M.B., Gobeil, C., 1998. A sediment and organic carbon budget for the Canadian Beaufort Shelf. Mar. Geol. 144, 255–273. https://doi.org/10.1016/S0025-3227(97)00106-0

Martens, J., Romankevich, E., Semiletov, I., Wild, B., van Dongen, B., Vonk, J., Tesi, T., Shakhova, N., Dudarev, O.V., Kosmach, D., Vetrov, A., Lobkovsky, L., Belyaev, N., Macdonald, R.W., Pieńkowski, A.J., Eglinton, T.I., Haghipour, N., Dahle, S., Carroll, M.L., Åström, E.K.L., Grebmeier, J.M., Cooper, L.W., Possnert, G., Gustafsson, Ö., 2021. CASCADE – The Circum-Arctic Sediment CArbon DatabasE. Earth Syst Sci Data 13, 2561–2572. https://doi.org/10.5194/essd-13-2561-2021

Martens, J., Wild, B., Pearce, C., Tesi, T., Andersson, A., Bröder, L., O'Regan, M., Jakobsson, M., Sköld, M., Gemery, L., 2019. Remobilization of old permafrost carbon to Chukchi Sea sediments during the end of the last deglaciation. Glob. Biogeochem. Cycles 33, 2–14.

Rantanen, M., Karpechko, A.Y., Lipponen, A., Nordling, K., Hyvärinen, O., Ruosteenoja, K., Vihma, T., Laaksonen, A., 2022. The Arctic has warmed nearly four times faster than the globe since 1979. Commun. Earth Environ. 3, 1–10. https://doi.org/10.1038/s43247-022-00498-3

Ruff, M., Fahrni, S., Gäggeler, H., Hajdas, I., Suter, M., Synal, H., Szidat, S., Wacker, L., 2010. On-line radiocarbon measurements of small samples using elemental analyzer and MICADAS gas ion source. Radiocarbon 52, 1645–1656.

Schirrmeister, L., Froese, D., Tumskoy, V., Grosse, G., Wetterich, S., 2013. Yedoma: Late Pleistocene ice-rich syngenetic permafrost of Beringia. Encycl. Quat. Sci. 2nd Ed. 542–552.

Schuur, E. a. G., McGuire, A.D., Schädel, C., Grosse, G., Harden, J.W., Hayes, D.J., Hugelius, G., Koven, C.D., Kuhry, P., Lawrence, D.M., Natali, S.M., Olefeldt, D., Romanovsky, V.E., Schaefer, K., Turetsky, M.R., Treat, C.C., Vonk, J.E., 2015. Climate change and the permafrost carbon feedback. Nature 520, 171–179. https://doi.org/10.1038/nature14338

Shearer, J., 1971. Preliminary interpretation of shallow seismic reflection profiles from the west side of Mackenzie Bay, Beaufort Sea. Rep. Act. Part B Geol. Surv. Can. Pap. 71–1.

Stuiver, M., Polach, H.A., 1977. Discussion reporting of 14C data. Radiocarbon 19, 355–363.

Tarnocai, C., Canadell, J.G., Schuur, E. a. G., Kuhry, P., Mazhitova, G., Zimov, S., 2009. Soil organic carbon pools in the northern circumpolar permafrost region. Glob. Biogeochem. Cycles 23. https://doi.org/10.1029/2008GB003327

Vonk, J.E., Semiletov, I.P., Dudarev, O.V., Eglinton, T.I., Andersson, A., Shakhova, N., Charkin, A., Heim, B., Gustafsson, Ö., 2014. Preferential burial of permafrost-derived organic carbon in S iberian- A rctic shelf waters. J. Geophys. Res. Oceans 119, 8410–8421. https://doi.org/10.1002/2014JC010261

Wu, J., Mollenhauer, G., Stein, R., Köhler, P., Hefter, J., Fahl, K., Grotheer, H., Wei, B., Nam, S.-I., 2022. Deglacial release of petrogenic and permafrost carbon from the Canadian Arctic impacting the carbon cycle. Nat. Commun. 13, 7172. https://doi.org/10.1038/s41467-022-34725-4